3-2016

Quantification of Warming Climate-Induced Changes in Terrestrial Arctic River Ice Thickness and Phenology

Hotaek Park

Yasuhiro Yoshikawa

Kazuhiro Oshima

Youngwook Kim

Thanh Ngo-Duc

See next page for additional authors

Recommended Citation

Park, H., Y. Yoshikawa, K. Oshima, Y. Kim, T. Ngo-Duc, J. Kimball, and D. Yang, 2016: Quantification of Warming Climate-Induced Changes in Terrestrial Arctic River Ice Thickness and Phenology. J. Climate, 29, 1733–1754, doi: 10.1175/JCLI-D-15-0569.1

Quantification of Warming Climate-Induced Changes in Terrestrial Arctic River Ice Thickness and Phenology

HOTAEK PARK,* YASUHIRO YOSHIKAWA,+ KAZUHIRO OSHIMA,* YOUNGWOOK KIM,#
THANH NGO-DUC,@ JOHN S. KIMBALL,# AND DAQING YANG&

* *Institute of Arctic Climate and Environment Research, JAMSTEC, Yokosuka, Japan*
+ *Department of Civil and Environmental Engineering, Kitami Institute of Technology, Kitami, Hokkaido, Japan*
# *Numerical Terradynamic Simulation Group, College of Forestry and Conservation, University of Montana, Missoula, Montana*
@ *Department of Meteorology and Climate Change, Hanoi College of Science, Vietnam National University, Hanoi, Vietnam*
& *National Hydrology Research Centre, Environment Canada, Saskatoon, Saskatchewan, Canada*

(Manuscript received 12 August 2015, in final form 11 December 2015)

ABSTRACT

A land process model [the coupled hydrological and biogeochemical model (CHANGE)] is used to quantitatively assess changes in the ice phenology, thickness, and volume of terrestrial Arctic rivers from 1979 to 2009. The CHANGE model was coupled with a river routing and discharge model enabling explicit representation of river ice and water temperature dynamics. Model-simulated river ice phenological dates and thickness were generally consistent with in situ river ice data and landscape freeze–thaw (FT) satellite observations. Climate data indicated an increasing trend in winter surface air temperature (SAT) over the pan-Arctic during the study period. Nevertheless, the river ice thickness simulations exhibited a thickening regional trend independent of SAT warming, and associated with less insulation and cooling of underlying river ice by thinning snow cover. Deeper snow depth (SND) combined with SAT warming decreased simulated ice thickness, especially for Siberian rivers, where ice thickness is more strongly correlated with SND than SAT. Overall, the Arctic river ice simulations indicated regional trends toward later fall freezeup, earlier spring breakup, and consequently a longer annual ice-free period. The simulated ice phenological dates were significantly correlated with seasonal SAT warming. It is found that SND is an important factor for winter river ice growth, while ice phenological timing is dominated by seasonal SAT. The mean total Arctic river ice volume simulated from CHANGE was 54.1 km^3 based on the annual maximum ice thickness in individual grid cells, while river ice volume for the pan-Arctic rivers decreased by 2.82 km^3 (0.5%) over the 1979–2009 record. Arctic river ice is shrinking as a consequence of regional climate warming and coincident with other cryospheric components, including permafrost, glaciers, and sea ice.

1. Introduction

Arctic river ice is one of the major components of the global cryosphere and has a distinctive seasonal phenology characterized by freezeup and growth during fall and winter, followed by breakup with the onset of spring thawing and the seasonal flood pulse. This seasonality is closely related to atmospheric heat fluxes. Arctic warming that was significant over the past several decades (Bekryaev et al. 2010) has resulted in changes in seasonal river ice phenology, characterized by decreases in ice thickness and earlier ice breakup (Magnuson et al. 2000; Vuglinsky 2006; Lesack et al. 2014; Shiklomanov and Lammers 2014). In cold Arctic rivers, ice growth depends on surface air temperature (SAT) during the cold season but is also affected by the insulating effect of winter snow cover (Prowse and Beltaos 2002). Thinner snow accumulation through the winter may enhance the growth of river ice. A decreasing trend in winter snow depth (SND) has been observed in the terrestrial Arctic during recent decades (IPCC 2013), particularly for North America (Dyer and Mote 2006; Park et al. 2012). Conversely, long-term in situ SND observations in Eurasia show an increasing trend (Bulygina et al. 2009). These contrasting

Corresponding author address: Hotaek Park, Institute of Arctic Climate and Environment Research, JAMSTEC, 2-15 Natsushimacho, Yokosuka 237-0061, Japan.
E-mail: park@jamstec.go.jp

DOI: 10.1175/JCLI-D-15-0569.1

snow cover changes may promote divergent trends in river ice phenology as a result of associated regional differences in surface insulation. However, Shiklomanov and Lammers (2014) documented that in situ observations at Russian river mouths where ice thickness decreased had not revealed any significant correlation between ice thickness and SND.

Seasonal snowmelt in the Arctic typically begins with SAT warming in the spring. The timing of snow cover depletion is dependent on multiple factors, though a thinner snowpack generally disappears more rapidly in the spring. A regional trend toward earlier snowpack depletion has been observed in the terrestrial Arctic (Kim et al. 2015). Earlier snow cover retreat in the spring reduces ice albedo and therefore enhances the decay of river ice (Gray and Prowse 1993). Earlier snowmelt, runoff, and the spring flood pulse from surrounding uplands also likely weaken and break up river ice earlier (Rawlins et al. 2005; Lesack et al. 2014). While a thicker snowpack may maintain a higher surface albedo and delay melting of underlying ice in the spring, it increases runoff and river discharge from additional snowmelt, promoting rapid river ice breakup once thawing is underway. Bieniek et al. (2011) found that increased winter snow cover in Alaska contributed to earlier ice breakup by increasing spring river discharge. Previous studies thus provide conflicting reports regarding the role of snow cover on river ice phenology.

Most previous studies on Arctic river ice phenology have used in situ observations made at either river mouths or other specific locations within river basins. If geomorphic and climatic heterogeneities of observation sites are considered, in situ observations are limited in terms of expanding to regional or global scales. Satellite observational data have been widely used to examine changes in seasonal ice phenology (i.e., freezeup and breakup dates) from local to regional scales (Gatto 1990; Murphy et al. 2001; Pavelsky and Smith 2004; Vincent et al. 2004). However, the inability of current satellite observations to accurately determine snow and ice thicknesses inherently limits their application to studies of winter ice processes underlying snow cover. These limitations may be partially mitigated through numerical modeling. A number of models have been developed that have simulated ice freezeup and breakup dynamics on various rivers (Beltaos 1997; Ma and Fukushima 2002; Prowse and Conly 1998; Yoshikawa et al. 2014). However, most of these models have focused on relatively short river reaches and small areas.

During the past decades, a number of attempts have been made to quantify changes in cryospheric components over polar and high-latitude regions of the globe (Lemke et al. 2007). These assessments tended to point to changes in Arctic sea ice and Greenland ice sheet dynamics, because of their large influence on regional and global climate. Although the influence of river ice on climate may be relatively smaller, the importance of river ice to biogeochemical and socioeconomic systems has been widely recognized, especially at local-to-regional scales (Prowse and Beltaos 2002). As mentioned above, recent climate change has coincided with large apparent changes in river ice phenology. To date, however, very few studies have provided quantitative assessments of the areal extent and volume of the ice (Brooks et al. 2013) and associated changes in ice phenology for terrestrial Arctic rivers, including potential changes from recent climate warming.

The main objective of this study was to quantitatively assess changes in terrestrial Arctic river ice phenology, including ice volume, thickness, and annual freezeup and breakup dates during the period 1979–2009. The assessment was made by using an improved coupled hydrological and biogeochemical process model (CHANGE; Park et al. 2011) integrated with a river routing and discharge model that includes river ice and water temperature T_w dynamics. We also conducted a model sensitivity study to delineate factors affecting

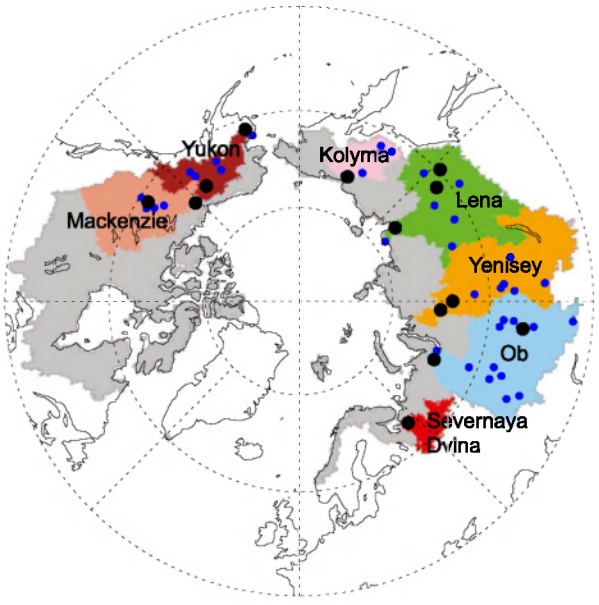

FIG. 1. The seven major Arctic watersheds and river systems used for model evaluations in this study. Gray areas represent other remaining pan-Arctic watersheds. Black dots represent river mouth locations for the seven watersheds and upstream hydrological stations used for evaluating model simulations. Blue dots represent subbasin outlet locations used for assessing contributions of the basins to the estimated total river ice volume over all pan-Arctic rivers.

river ice growth and breakup diagnosed by model experiments using several scenarios that incorporated different climatic forcings. The model was applied over the entire terrestrial Arctic river system, including Hudson Bay rivers (Fig. 1). The simulated hydrological variables (e.g., discharge, ice thickness, and T_w) were compared with available in situ observations at the mouths and upstream stations of the major pan-Arctic river basins (Fig. 1). A satellite microwave remote sensing record of landscape freeze–thaw (FT) seasonal dynamics was also used to verify simulated Arctic river ice phenological dates in relation to satellite-observed changes in landscape frozen and nonfrozen conditions at the pan-Arctic scale.

2. Model description

a. Land surface model

CHANGE (Park et al. 2011) is a state-of-the-art process-based model that calculates heat, water, and carbon fluxes in the atmosphere–land system, soil thermal and hydrologic states, snow hydrology, and plant stomatal physiology and photosynthesis. Park et al. (2011) provide a detailed description of the CHANGE model, while model elements pertaining to this study are summarized below. CHANGE numerically solves the heat and hydraulic conduction equations and represents permafrost dynamics, including an explicit treatment of soil FT phase transitions over up to 50.5 m of soil depth. A two-layer energy and mass balance approach is used to simulate snow accumulation and snowmelt at the land surface. The energy balance includes snowmelt, refreezing, and changes in the snowpack heat content. The water mass balance represents snow accumulation/ablation, changes in snow water equivalent, and water yield from the snowpack. The snowpack is compacted by snow/ice metamorphism and overburden, affecting snow density. The calculated snow density and snow water equivalent determine the thickness of the snowpack.

Water at the soil surface is split between soil infiltration and surface runoff. The vertical water flux between soil column layers is numerically solved with Darcy's law. If the surface soil layer becomes saturated, excess surface water is determined as surface runoff. For lower soil layers, CHANGE routes excess soil moisture to deeper soil layers; this assumes that excess soil moisture may flow laterally over land within a grid cell but would eventually move down through the soil layers, resulting in excess groundwater in lower soil layers. If the bottom soil layer becomes saturated, the excess groundwater is added to the subsurface runoff. When permafrost is present within the soil column, water infiltration to lower soil layers is considerably impeded. In CHANGE, this process is represented with a parameterization for soil ice impedance.

b. River discharge model

We coupled the river routing scheme Total Runoff Integrating Pathways (TRIP2; Ngo-Duc et al. 2007) to CHANGE to represent basin runoff routing and river discharge dynamics. TRIP2 is a storage-based gridcell-wise routing model and is based on spatially effective subgrid parameters that act to broadly represent a more realistic travel time. TRIP2 passes surface and subsurface runoff calculated by CHANGE directly to individual storage reservoirs where water is routed to the river mouth through a prescribed channel network of 0.5° spatial resolution (Oki and Sud 1998). The contribution of groundwater to streamflow is represented by a linear function of outflow discharge with a groundwater delay factor parameter that depends on the soil type and geology of the grid cell (Arora and Boer 1999). TRIP2 has been successfully tested in relation to observed runoff for the major global basins (Ngo-Duc et al. 2007; Pappenberger et al. 2010).

In this study, the water balance of the surface storage within a grid cell S_s in TRIP2 was improved by adding a river ice effect:

$$\frac{dS_s}{dt} = D_U + D_{O,g} + D_{I,s} - \left(\frac{v}{l \times p_m} \times S_s\right) + \left(\frac{dh_i}{dt} \times l \times W\right) \quad (1)$$

where t is time step (s); D_U is total inflow ($m^3 s^{-1}$) from upstream grid boxes; $D_{O,g}$ is outflow ($m^3 s^{-1}$) from the groundwater reservoir; $D_{I,s}$ is surface runoff ($m^3 s^{-1}$) calculated by CHANGE; v is the velocity; l is the river channel length within the grid box calculated geometrically; p_m is the meandering ratio, which adjusts the river length; h_i is the ice thickness calculated by the river ice model (Yoshikawa et al. 2014); and W is river width that has a geomorphological relationship with mean annual runoff (Arora and Boer 1999). The fifth term on the right-hand side of Eq. (1) represents the change of water volume resulting from changes in ice thickness. A detailed description of the TRIP2 model is also found in Ngo-Duc et al. (2007).

c. River ice thickness and water temperature

Once seasonal ice cover in cold rivers is established, ice growth during the winter is primarily dependent on vertical downward freezing severity from the atmosphere. Snow cover decouples surface air and river ice

TABLE 1. Summary of the model experiments used in this study.

Name	Description of treatment	
	Air temperature	Precipitation
CTRL	—	—
US_{O_M}	—	20% added to precipitation during Oct–Mar
UT_{O_M}	3°C added to air temperature during Oct–Mar	—
UT_{A_M}	2°C added to air temperature during Apr–May	—
$USDT_{O\_M}$	3°C subtracted from air temperature during Oct–Mar	20% added to precipitation during Oct–Mar
$US_{O\_M}UT_{A\_M}$	3°C added to air temperature during Apr–May	20% added to precipitation during Oct–Mar
$DS_{O\_M}UT_{A\_M}$	2°C added to air temperature during Apr–May	20% subtracted from precipitation during Oct–Mar
$DSUT_{O\_M}$	2°C added to air temperature during Oct–Mar	20% subtracted from precipitation during Oct–Mar
DS_{O_M}	—	20% subtracted from precipitation during Oct–Mar
DT_{O_M}	3°C subtracted from air temperature during Oct–Mar	—
DT_{A_M}	2°C subtracted from air temperature during Apr–May	—
SEN_EXP[a]	1°C altered during Oct–Mar ranging from −3 to +3°C	10% altered during Oct–Mar ranging from −30 to +30%

[a] The treatment for the sensitivity runs (SEN_EXP) was made independently to individual variables SAT and SND.

thermal conditions, leading to significant impacts on river ice growth underlying the surface snow cover. Yoshikawa et al. (2014) presented a model to estimate river ice thickness on the basis of heat exchanges between atmosphere–snow–ice–frazil ice–water boundaries using relatively few input variables, such as SAT, T_w, and effective water depth. The model includes two important parameters that represent processes relating to ice sheet formation and melting, where SAT and snow cover are the major process-related variables. Here, snow cover overlying the river ice layer is represented by SND of the same land grid cell calculated by CHANGE.

In a well-mixed river, distributions of T_w and depth-averaged frazil ice concentration along the river can be described by the one-dimensional advection–diffusion equation. The magnitude of upward advection, diffusion, and heat flux from flowing water to the bottom of the river ice layer is relatively small (Yoshikawa et al. 2014). The terms were thus removed from the basic advection–diffusion equation, which was rewritten in a simpler form to calculate river T_w dependent on SAT and effective water depth. A full description of the river ice and T_w model is given in Yoshikawa et al. (2014).

3. Data and methodology

a. Meteorological forcing data and simulations

We used gridded climatic forcing data for the model simulation, which has a global 0.5° latitude/longitude spatial resolution and 3-h time step covering the 1979–2009 study period [WATCH Forcing-Data ERA-Interim (WFDEI); http://www.eu-watch.org/data_availability; see Weedon et al. 2014]. ERA-Interim surface meteorology data (e.g., temperature, surface pressure, specific humidity, and downward longwave radiation) were used as baseline information for the WFDEI. The ERA-Interim data were interpolated at half-degree spatial resolution, consistent with the land–sea mask defined by the Climatic Research Unit (CRU). Additional corrections for elevation and monthly bias of climatic trends in the ERA-Interim variables were applied to the interpolated data. The WFDEI precipitation data were generated using two datasets: the Global Precipitation Climatology Centre full product (GPCCv5) and CRU Time Series version 3.10 (CRU TS3.1) (Weedon et al. 2014). The GPCCv5 was used to correct monthly ERA-Interim precipitation totals, and the monthly number of ERA-Interim precipitation days was adjusted for consistency with the CRU data. Undercatch corrections to the precipitation gauge data were made following Adam and Lettenmaier (2003), who provided separate average calendar monthly catch ratios for rainfall and snowfall rates for each half-degree grid cell to adjust precipitation rates to allow for the effects of orography (Adam et al. 2006).

A static land cover classification was used for the model simulations, as defined from a global land cover map (Ramankutty and Foley 1999), while the vegetation phenology was prognostic based on estimated carbon and nitrogen fluxes (Thornton and Zimmermann 2007). Vertical soil texture fractions for sand, silt, and clay derived from the IGBP SoilData System were used in the model to estimate soil thermal and hydraulic properties, in combination with simulated soil organic matter at each time step.

Different sets of model sensitivity experiments were designed to diagnose how changes in SND and SAT affect estimated river ice thickness and phenology. The model experiments were based on 11 scenarios, including a control run (CTRL) that used the original

forcing dataset (Table 1). To assess the influence of SND and/or SAT changes on river ice thickness, precipitation was adjusted by ±20% from the baseline forcing data for the snowfall season (i.e., October–March); SAT inputs were adjusted by ±3°C during the same period, and the SAT treatment was, in turn, combined with the modified winter precipitation. SAT in the spring (April–May) was adjusted by ±2°C to examine associated temperature impacts on estimated river ice breakup. The model sensitivity experiments excluded the influence of SAT on associated precipitation partitioning between snowfall and rainfall. In the above experiments, the temperature treatments were derived from standard deviations of the monthly temperatures from the reanalysis data [e.g., ERA-Interim, CFS Reanalysis (CFSR), and Japanese 55-year Reanalysis Project (JRA-55)], averaged over the major Arctic river basins (Fig. 1) for the 1979–2009 record. The precipitation treatments represent the percentage of the standard deviation to monthly mean values of precipitation datasets (e.g., GPCP and CMAP) derived for the same area and period as temperature data. Additional experiments were also made to assess the sensitivity of model-estimated maximum ice thickness to the SAT and SND adjustments. A series of six model sensitivity runs for respective SAT and SND predictions was carried out for the 1979–2009 period. In each model run, SAT and SND were adjusted by ±1°C and ±10%, and ±3°C and ±30% from their original cold season values (i.e., October–March).

b. *In situ datasets for model validation*

Benson and Magnuson (2012) compiled observational data on ice phenological and physical properties for 865 lakes and rivers in the Northern Hemisphere. The resulting Global Lake and River Ice Phenology Database consists of seasonal ice thickness, with beginning and ending dates for river ice from the mouths of the major Arctic river basins (Fig. 1). The data records extend from 1845 to the 2000s, but with variable record lengths for individual stations. We used the observational data extending from 1979 for validating the CHANGE model-simulated ice regime and associated long-term variability in ice phenology for these rivers. River ice thickness data for the 1979–2008 period from a single upstream station in each of the Yenisey and Lena Rivers were collected by the Russian State Hydrological Institute (SHI) and also used for model validation.

A Eurasian river T_w dataset was compiled by Lammers et al. (2007), covering 20 stations with data records extending from the mid-1930s to the early 1990s (http://data.eol.ucar.edu/codiac/dss/id=106.233); the available records extending from 1979 and observed at the mouths of the five major Eurasian river basins (Fig. 1) were used to assess the corresponding model-simulated T_w dynamics. Yang et al. (2014) compiled a T_w observation dataset for the Mackenzie River, made at various locations and times by Canadian government agencies. All available T_w data observed at the Mackenzie basin Arctic Red River station from 1979–2009 were used for this study.

Daily river discharge records for the major Eurasian river watersheds and their upstream stations from 1979 to 2008 were obtained from the University of New Hampshire data repository, the Arctic Rapid Integrated Monitoring System (ArcticRIMS; http://rims.unh.edu), and SHI, respectively. The U.S. Geological Survey observes discharges at the basin outlet and upstream gauging stations of the Yukon River basin, where daily observational data from two major tributary stations (IDs: 15565447 and 15356000) were obtained with records from 1975–2010. The daily discharge measurements for the Mackenzie Arctic Red River and Liard River sites were obtained from the Canadian hydrometric database (HYDAT) for the period 1973–2011. The river discharge data for the major Arctic watersheds (Fig. 1) were used to evaluate CHANGE-simulated discharge at the river outlets over the 1979–2008 record, except for the Kolyma River with the smaller 1979–94 period.

We used a global Earth System Data Record (ESDR; http://dx.doi.org/10.5067/MEASURES/CRYOSPHERE/nsidc-0477.003) of daily landscape FT status derived from satellite microwave remote sensing to define primary thaw and frozen dates over all vegetated land areas within the pan-Arctic basin for the 1979–2009 study period (Kim et al. 2012). Barren land, including permanent ice and snow, and grid cells with 20% or greater proportional open water body coverage were excluded from the FT classification. The FT-ESDR was derived from a temporal classification of 37-GHz vertically polarized brightness temperature records and provides a daily classification of the predominant frozen or nonfrozen status of the land surface within each 25-km grid cell (Kim et al. 2012). The FT signal from satellite microwave remote sensing is sensitive to seasonal changes in the abundance and mobility of liquid water in the landscape, including the timing of seasonal snowmelt and the spring flood pulse in Arctic rivers (Kimball et al. 2001; Rawlins et al. 2005). As an independent reference, annual timing of primary spring thaw and fall freeze dates determined from the FT-ESDR were compared against CHANGE model-simulated timing of river ice breakup and freezeup over the pan-Arctic domain. The primary seasonal thaw date within each

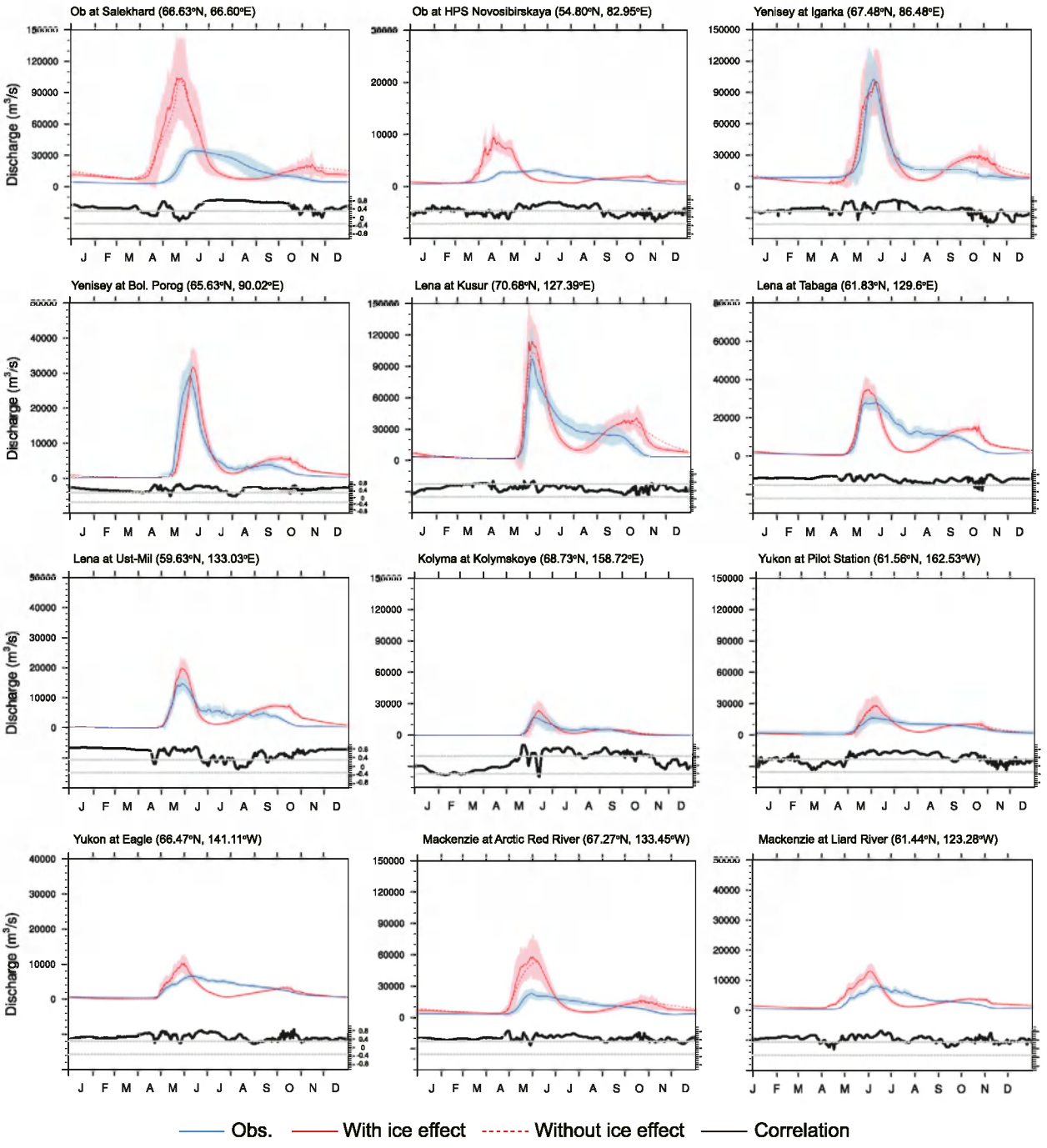

FIG. 2. Daily discharges simulated by CHANGE (red) compared to observations (blue) at the mouths and upstream stations of the major Arctic rivers. Two sets of daily discharge simulations are represented, including river ice effects (red line) and without representing river ice (red dashed line). The daily discharges were averaged from 1979–2008, except for Kolyma, which was averaged from 1979–94; blue and red shades denote one temporal standard deviation ranges. The bold black lines represent daily correlation coefficients between observations and simulations for the available periods within individual watersheds; dotted gray lines denote a 90% significance level.

grid cell was determined as the first day for which 12 out of 15 consecutive days from January to June were classified as nonfrozen from the daily FT-ESDR (Kim et al. 2014). A similar method was used to determine the primary seasonal freezeup date from the FT-ESDR for which 12 of 15 consecutive days were classified as either transitional or frozen between September and December.

4. Results

a. Comparison between CHANGE simulations and independent observations

1) DISCHARGE

Figure 2 compares the simulated daily mean discharge with observations at gauging stations closest to the river mouths of the six major pan-Arctic watersheds (e.g., Ob, Yenisey, Lena, Kolyma, Yukon, and Mackenzie) and at their upstream stations, with the daily correlation coefficients between observations and simulations. In the model and data comparisons, two simulation sets are represented: a model baseline simulation that includes the effect of river ice on discharge, and a second simulation that excludes the ice effect. The model river ice treatment generally captured the influence of ice on seasonal river discharge, with rising water levels in the autumn when the ice begins to form, and the spring flood pulse and river ice breakup period. The baseline simulations favorably compare at the 90% significance level with the observations during the growing season from May to September in most of the watersheds, although intermittent periods of weaker model agreement with the observations were also identified (Fig. 2). The model-simulated spring peak discharges are generally consistent with the observations; the agreement tends to improve at upstream stations of smaller basin scale relative to the river mouths. However, the model shows apparent overestimation of spring peak discharge for the Ob and Mackenzie Rivers as reported by Slater et al. (2007), which is attributed to relatively higher snowmelt and runoff inputs in these basins. The CHANGE simulations showed apparent overestimation of winter SND in western Siberia (Park et al. 2012) because of overestimation of cold season precipitation (Decharme and Douville 2006). A portion of the Ob (11.0% of basin area; Yang et al. 2004) and Mackenzie (48.9% of basin area; Yang et al. 2014) basins is covered by wetlands and lakes that reduce runoff and peak river discharge rates. Model deficiencies in representing wetland and lake processes in CHANGE may also be a cause of the apparent model overestimation of peak discharge relative to the basin observations.

CHANGE simulated faster water release across all basins following seasonal peak flows, resulting in relatively lower summer base flows than the observations. The lower summer discharge is conversely attributed to underestimation of the gridded observation-based precipitation forcing (Serreze et al. 2002; Adam and Lettenmaier 2003), especially in mountainous regions

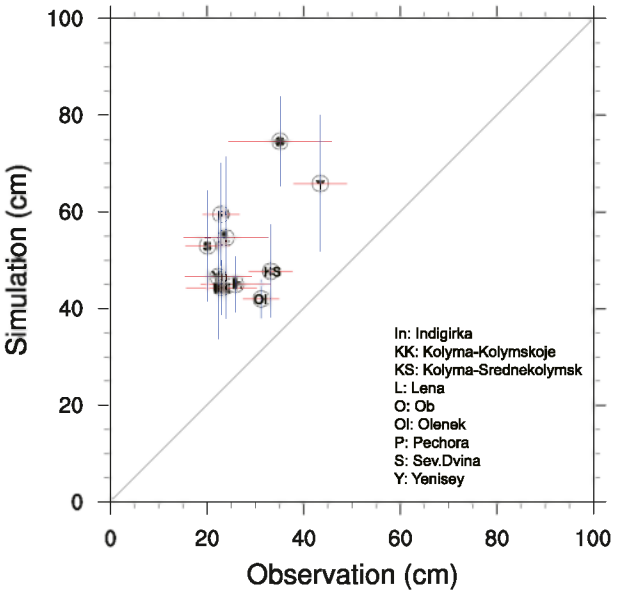

FIG. 3. Comparison of observed and simulated winter (January–March) mean snow depth at the mouths of the major Arctic watersheds. Red (horizontal) and blue (vertical) lines represent standard deviations of the observations and simulations, respectively.

(Hatta et al. 2009). CHANGE tends to overestimate active layer thickness (Park et al. 2013a), which increases soil water storage capacity. Under less summer precipitation, the larger bias in model soil water holding capacity likely propagates to lower subsurface runoff and base flow. CHANGE also tends to overestimate leaf area index derived as a function of simulated leaf carbon and nitrogen, likely resulting in higher evapotranspiration losses and thus less runoff and streamflow. The model simulations do not account for streamflow regulation from impoundments and artificial reservoirs established within all of the watersheds examined, which likely contribute to differences between the model discharge simulations and observations. The lack of impoundments in the model simulations likely contributes to higher seasonal flood peaks, faster declining limbs, and generally faster water routing from the basins relative to the observations (Su et al. 2005).

2) SNOW DEPTH

A Russian river ice dataset (Lammers et al. 2007) includes three-times-per-month SND observations over river ice cover at the river mouths of major watersheds (Fig. 1). The SND observations were averaged from January to March for individual years over the available record from 1979. A distance-weighted average of model SND simulations for the four closest grid cells surrounding the river mouth locations was conducted

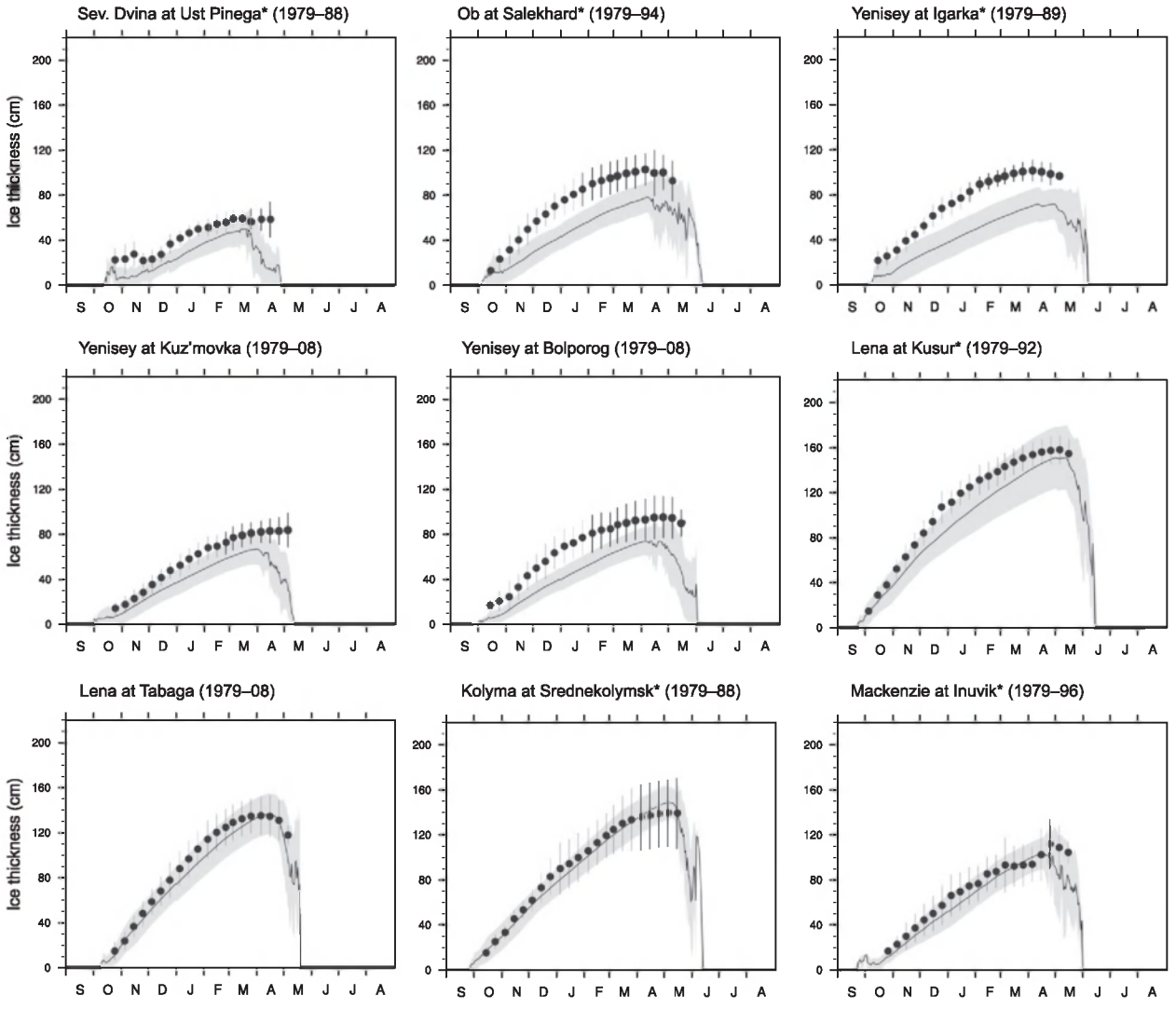

FIG. 4. Simulated daily river ice thicknesses (lines) compared to available observations (dots) at the mouths and upstream stations of the major Arctic rivers. The comparisons were made for the periods during which observations were available for individual watersheds. The shading and vertical lines on the dots denote one standard deviation ranges.

consistent with the SND observation periods. A comparison of observed and simulated SND dynamics for the river mouths of the major Russian watersheds is shown in Fig. 3. The SND simulations were based on a model calculation of land areas within a grid cell. The model results show apparent SND overestimation relative to the observations. The model SND overestimation was more significant in western Siberia than in the eastern areas. In the Ob and Yenisey, the simulated SND was 2 or more times greater than the SND observations. Differences between the model SND simulations and observations may reflect differences in surface roughness and microclimate between river ice and adjacent land areas, which are not adequately represented in the model. The model overestimation of SND may also increase uncertainties for the simulation of river ice thickness.

3) ICE THICKNESS AND PHENOLOGY

The CHANGE-simulated seasonal river ice growth and decay dynamics were compared with independent ice thickness observations at the mouths of the six major Arctic rivers and at the upstream stations of the Yenisey and Lena Rivers (Fig. 4). The model results showed generally favorable performance in predicting the timing of maximum ice thickness at most locations (Fig. 4). The model simulations also generally captured the observed ice growth during the winter season. However, larger differences in winter ice growth between the model simulations and

TABLE 2. Correlation coefficient r and RMSE (days) differences between the observations and simulations for river ice breakup and freezeup dates at the river mouths of individual watersheds. Statistically significant correlations with 90% significance level are highlighted with bold font.

Characteristic		Severnaya Dvina	Ob	Yenisey	Lena	Kolyma
Breakup date	r	**0.76**	**0.90**	0.27	0.31	**0.74**
	RMSE	19.1	13.5	6.4	9.4	6.0
Freezeup date	r	0.29	0.37	**0.80**	**0.54**	**0.74**
	RMSE	19.4	17.1	5.0	15.3	6.6

observations were mainly found for stations where the model overestimated SND, especially in the Ob and Yenisey Rivers (Fig. 3). Thicker SND provides more effective insulation, resulting in thinner modeled river ice cover relative to lower SND levels or barren ice conditions. The deeper model SND levels within the watersheds also produced higher peak discharge simulations in those rivers relative to the observations (Fig. 2).

The simulated river ice breakup and freezeup dates were compared with observations at the Eurasian river mouths, which are summarized in Table 2. The highest correlation coefficients for ice breakup date are found for western Siberia rivers (i.e., Severnaya Dvina and Ob) and Kolyma, while eastern Siberia rivers (i.e., Yenisey, Lena, and Kolyma) show stronger correlations for freezeup dates. The model results showed generally larger errors [root-mean-square errors (RMSE)] in capturing the observed freezeup dates than the breakup dates (Table 2). The apparent differences between simulated and observed freezeup dates were attributed to model overestimation of river discharge during the fall season (Fig. 2). Higher river flows enhance turbulence, which can prolong the freezing-over process, thereby decreasing frazil ice generation (Beltaos and Prowse 2009).

Primary seasonal freeze and thaw dates of the regional landscape estimated from the satellite FT-ESDR observations were used as an additional observational benchmark to assess model performance in this study. The CHANGE-estimated annual (1979–2009) river ice breakup dates were significantly correlated ($p < 0.1$) with the FT-ESDR-derived primary spring thaw date over the pan-Arctic domain except for western Siberia and warmer southern subregions (Fig. 5a). The FT-ESDR results also exhibited an approximate 15-day delay in freezeup over the pan-Arctic domain relative to the CHANGE simulations, resulting in widespread

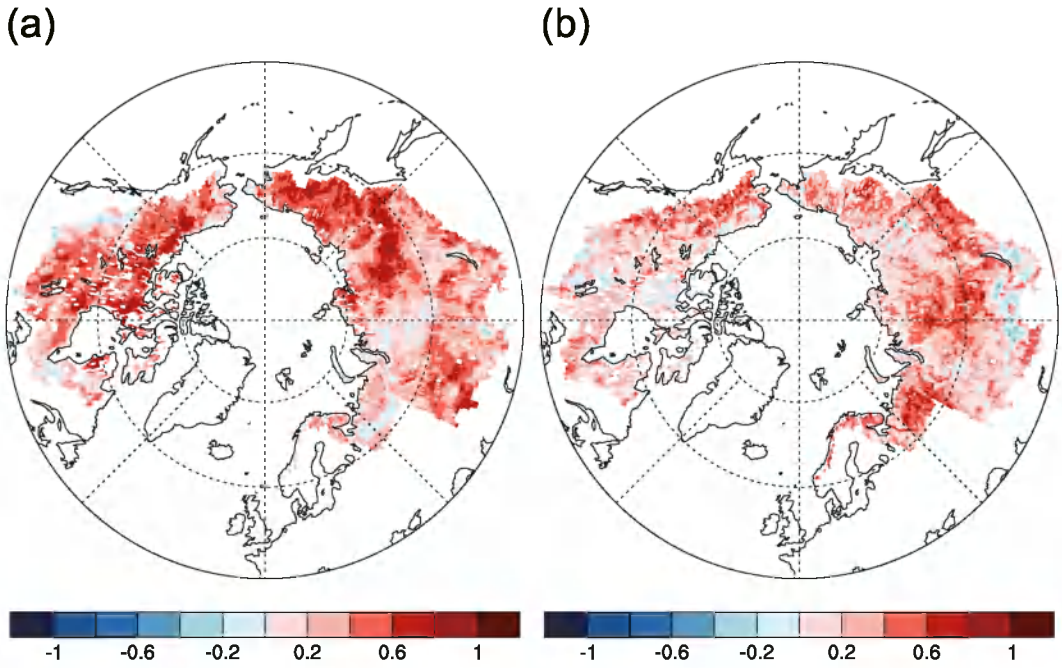

FIG. 5. The spatial distribution of correlation coefficient between CHANGE- and FT-ESDR-derived primary (a) thaw dates and (b) frozen dates for the 1979–2009 period. The correlation is significant where $r \geq |0.30|$.

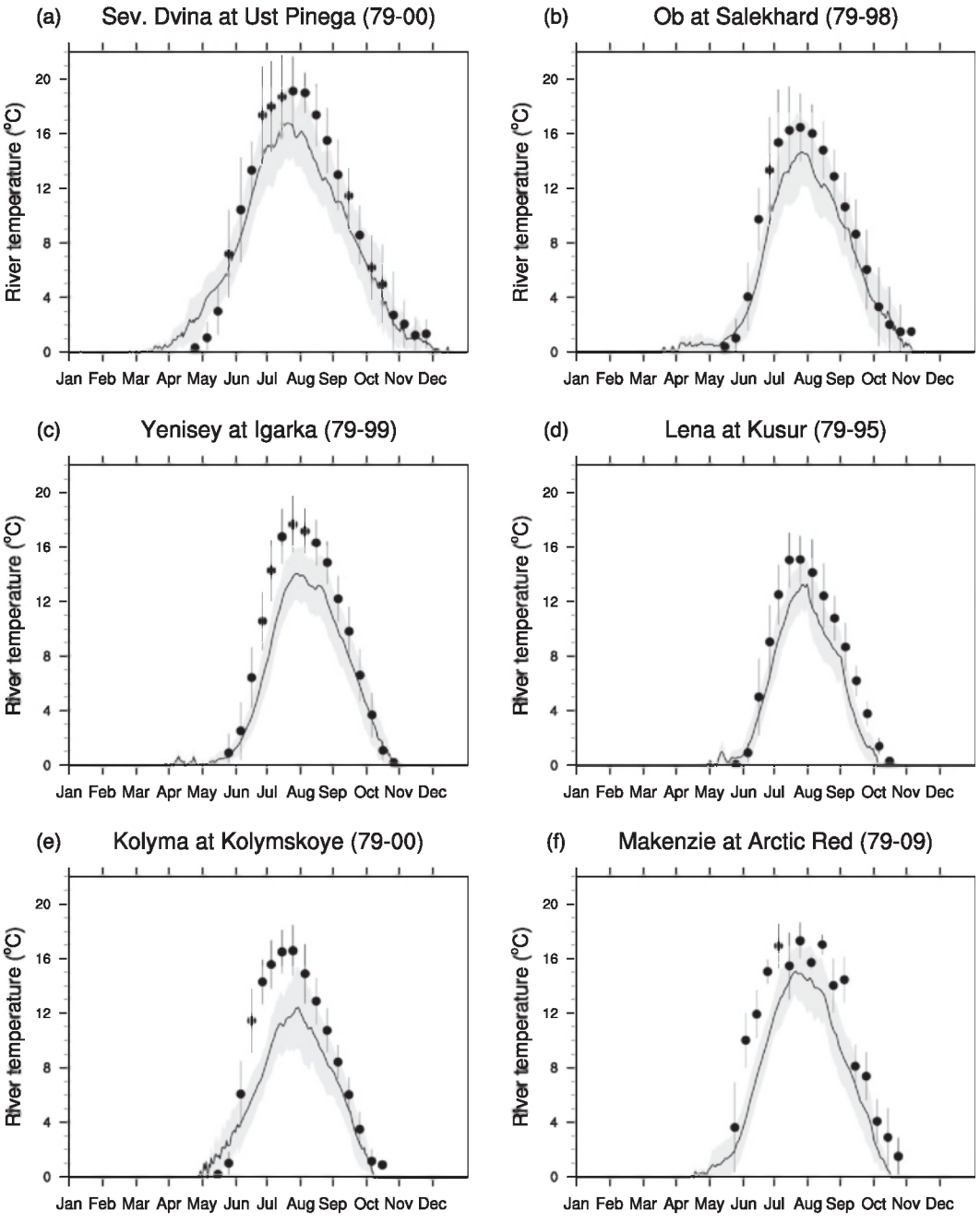

FIG. 6. Simulated daily river water temperatures (line) compared with available observations (dots) at the mouths of the major Arctic rivers. The comparisons were made for the periods that observations were available for individual watersheds. The shading and vertical lines on the dots denote one standard deviation ranges.

lower correlations in fall freezeup dates, except for portions of Siberia and Alaska (Fig. 5b). The spring thaw signal represented by the FT-ESDR is more closely tied with the timing of seasonal snowmelt and the spring flood pulse, directly impacting river ice breakup (Kimball et al. 2001; Rawlins et al. 2005; Semmens and Ramage 2013), which explains the closer FT-ESDR and CHANGE model agreement in the spring. In the autumn, the FT-ESDR is more closely associated with gradual freezing of surrounding land areas, which has less direct influence on river ice formation. The formation of river ice is also influenced by residual heat capacity and thermal buffering from groundwater and atmosphere stability needed for ice formation. These

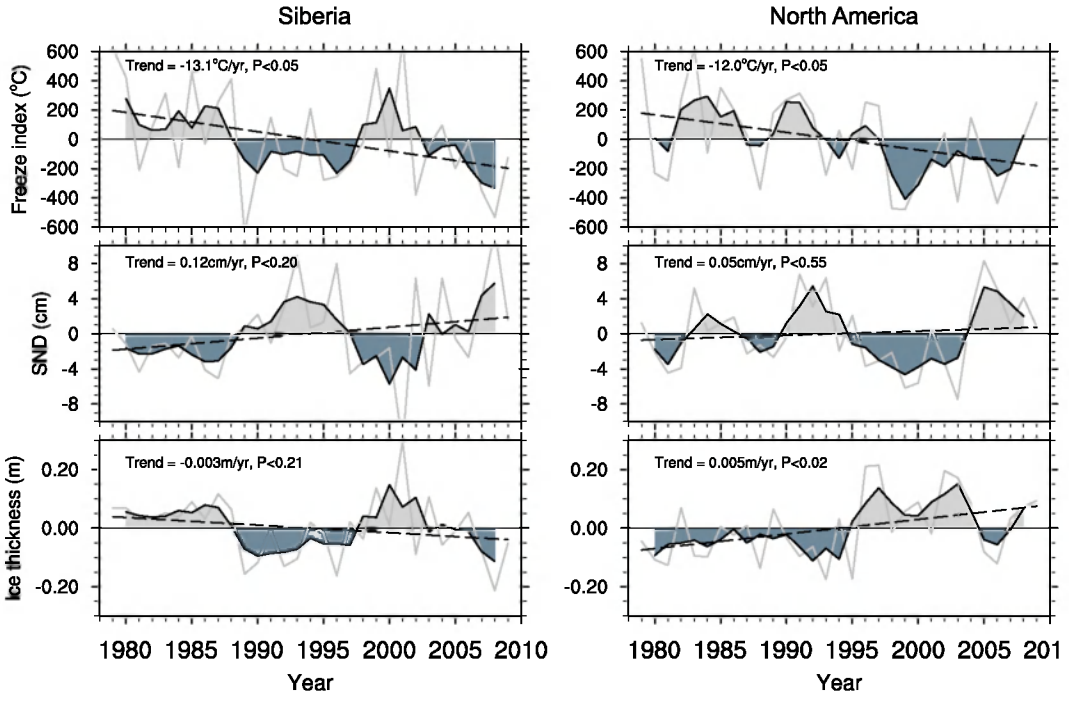

FIG. 7. Time series of (top) anomalous annual freezing index, (middle) snow depth from January to March, and (bottom) maximum river ice thickness in (left) Siberia (60°–73°N, 90°–135°E) and (right) North America (60°–73°N, 215°–260°E) rivers. The annual values of snow depth and maximum ice thickness represent model simulations rather than observations. In the figures, the light gray lines denote annual values; black lines denote 3-yr averages, and black dashed lines represent longer-term trends for the 1979–2009 simulation record.

factors are not directly represented by the coarse FT-ESDR footprint, which primarily represents a terrestrial landscape.

4) River water temperature

A notable CHANGE model improvement over earlier versions is the capability for T_w simulation at each grid cell along a basin flow network. The resulting T_w simulations were compared with observations from gauging stations closest to the outlets of the six Arctic river basins (Fig. 6). The T_w simulations and observations show similar seasonal variations in all locations, but a general model underestimation is apparent over the annual cycle, which is larger in summer than early spring and late autumn. The model underestimated observed summer T_w by 2°–5°C in most locations. Energy-budget-based stream temperature models are sensitive to the representation of river flow path-lengths, which may be degraded at the coarser spatial scales used for global model simulations (Wu et al. 2012). Model T_w accuracy may be improved by representing subgrid stream hydrography in the coarser model simulations. Van Vliet et al. (2012) reported that simulated T_w was highly sensitive to boundary conditions (i.e., headwater temperatures), which were improved as the model spatial resolution increased from ½° to ¼° and ⅛°.

b. Variability of river ice

1) Ice thickness

Figure 7 presents the annual anomalies of the freezing index defined as the accumulated degree-days below 0°C from October to April, the average estimated SND from January to March, and the estimated maximum river ice thickness in the Siberian (60°–73°N, 90°–135°E) and North American (60°–73°N, 215°–260°E) subregions. A warming temperature trend during the cold season reduced freezing intensity in the two subregions over the 1979–2009 record. The model SND simulations indicated increasing trends for the two regions, although they were not statistically significant ($p > 0.1$). The SND simulations show decadal variability, which is negatively correlated with estimated maximum river ice thickness for the two regions (e.g., $r = -0.84$, $p < 0.001$ in Siberia and $r = -0.55$, $p < 0.001$ in North America). In North America, for example, estimated river ice levels thickened from 1995 to 2005 despite warmer temperatures, indicating less snow insulation and ice cooling from SND thinning (Fig. 7). The simulated annual maximum

ice thickness of Siberian rivers was more strongly correlated with the model SND simulations ($r = -0.84, p < 0.001$) than the freezing index ($r = 0.81, p < 0.001$). The same tendency was found in North America, strengthening SND influences on estimated river ice growth.

Studies of historical trends for observed ice thickness reported that, since 1950, large Russian rivers have experienced a decrease in maximum ice thickness by -0.08 to $-1.3\,\mathrm{cm\,yr^{-1}}$ (Vuglinsky 2006; Shiklomanov and Lammers 2014). Our study quantifies a similar decrease of $-0.3\,\mathrm{cm\,yr^{-1}}$ in maximum ice thickness for Siberian rivers (Fig. 7). The estimated ice thickness in Fig. 7 represents a regional average for the defined Siberian and North American rivers, rather than specific locations. The use of regional anomalies can minimize the contribution of large biases from either specific grid cells or regions. Previous studies reporting observations at river mouths at the northernmost latitudes may represent somewhat larger trends for river ice thickness, because SAT warming trends in recent decades have been stronger in these regions (Screen and Simmonds 2010).

2) Ice phenology

Figure 8 shows the mean annual anomalies in estimated ice breakup and freezeup dates over the major Siberian and North American rivers within the pan-Arctic domain. The two continental subregions show later freezeup trends, coinciding with warmer autumn SAT (Bekryaev et al. 2010) that delays the timing and rate of ice formation. Changes in streamflow during late autumn and early winter also affect freezeup timing. Siberian rivers show generally increasing discharge trends in autumn and early winter (Smith et al. 2007). The combination of higher autumn streamflow and warmer SAT trends is likely contributing to the delay in estimated freezeup. In contrast, the later estimated freezeup trend was not significant ($p > 0.1$) for the North American rivers examined in this study.

The model-estimated river ice dynamics exhibit earlier breakup trends over the two continental subregions (Fig. 8). Beltaos and Prowse (2009) documented earlier ice breakup in North American rivers by 0.3–3 $\mathrm{days\,yr^{-1}}$ based on long-term observations, which is considerably earlier than our assessment by $-0.07\,\mathrm{days\,yr^{-1}}$ ($p < 0.37$) (Fig. 8). The simulated ice breakup trend in Siberian rivers was earlier by $0.23\,\mathrm{days\,yr^{-1}}$ ($p < 0.022$, Fig. 8), which is similar to previous reports of a 0.23–0.34 $\mathrm{days\,yr^{-1}}$ advance from 1980 to 2000 relative to the period from 1960 to 1980 in the rivers of northwestern European Russia (Vuglinsky 2006). Shiklomanov and Lammers (2014) reported earlier ice breakup trends from 0.03–0.09 $\mathrm{days\,yr^{-1}}$ at the mouths of Eurasian rivers over a 1955–2012 observation record. These previous studies concluded that the earlier ice breakup trends are strongly correlated with spring, rather than winter, SAT warming. The correlation between model-estimated ice breakup date and SAT partially includes the influence of river discharge on breakup timing. Increased spring flows tend to accelerate river ice breakup (Beltaos and Prowse 2009; Bieniek et al. 2011). In situ observation records indicate increased spring (May) discharge trends in Siberian rivers from 1979 to 2008 (Rawlins et al. 2009) that are likely contributing to the advance in ice breakup timing, as further discussed in section 4c below. Relatively strong regional trends toward earlier spring river ice breakup combined with weaker trends toward a delay in autumn ice formation result in a longer estimated annual ice-free period across the pan-Arctic domain. The longer ice-free seasonal trend is more significant in Siberia ($0.38\,\mathrm{days\,yr^{-1}}$, $p < 0.012$) than in North America ($0.19\,\mathrm{days\,yr^{-1}}$, $p < 0.14$).

3) Ice volume

The ice volume of each grid cell was calculated from the model-estimated maximum annual ice thickness and river length and width dimensions for the pan-Arctic rivers (Fig. 1). Figure 9 shows time series of the anomalous freezing index, averaged winter SND simulations, and the estimated integrated ice volumes over the pan-Arctic rivers (Fig. 1). The freezing index and SND results show decreasing annual trends averaged over the entire rivers. The estimated ice volume also indicates a decreasing trend ($-0.091\,\mathrm{km^3\,yr^{-1}}$, $p < 0.061$), but with large interannual variability ($\pm 3.0\,\mathrm{km^3}$ standard deviation) (Fig. 9). The averaged ice volume of the pan-Arctic rivers examined from 1979 to 2009 was $54.1 \pm 3.0\,\mathrm{km^3}$ with estimated river ice extent of $0.048 \times 10^6\,\mathrm{km^2}$. The total decrease in estimated ice volume over the 1979–2009 study period was $2.8\,\mathrm{km^3}$, which represented a 0.5% reduction from the long-term mean. Brooks et al. (2013) estimated $140\,\mathrm{km^3}$ and $0.12 \times 10^6\,\mathrm{km^2}$ for peak river ice volume and extent, respectively, over the Northern Hemisphere using a degree-day ice growth model based on the January freezing index. Both the CHANGE and degree-day model (Brooks et al. 2013) estimates indicate an average ice volume of $0.0012\,\mathrm{km^3}$ for a given $1\,\mathrm{km^2}$ ice area extent at annual maximum ice thickness.

An additional calculation of the annual maximum river ice volume was made using a degree-day ice growth model based on the Stefan equation (Brooks et al. 2013), with the freezing index from October to April (Fig. 9). The degree-day ice growth model also produced a decreasing trend in the estimated ice volume ($-0.075\,\mathrm{km^3\,yr^{-1}}$, $p < 0.015$). However, the CHANGE and degree-day model ice volume estimates exhibit

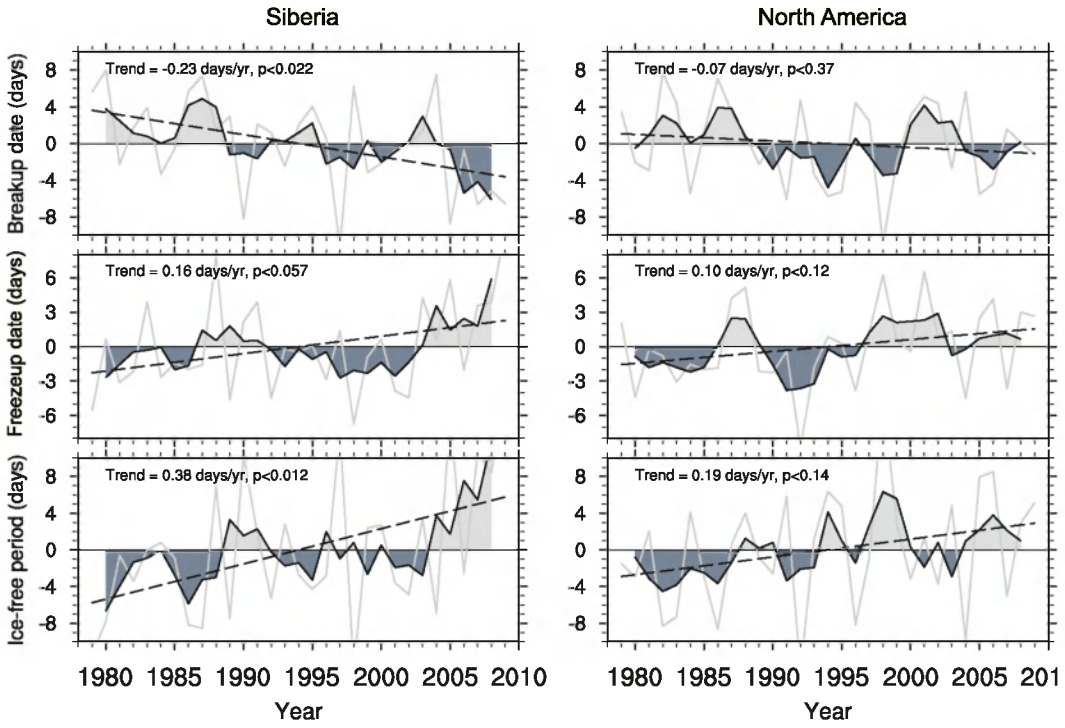

FIG. 8. Time series of (top) anomalous ice breakup date, (middle) freezeup date, and (bottom) ice-free duration in (left) Siberian (60°–73°N, 90°–135°E) and (right) North American (60°–73°N, 215°–260°E) rivers. The annual values of the three variables represent model simulations rather than observations. In the figures, the light gray lines denote annual values; the black lines denote 3-yr averages, and black dashed lines represent longer-term trends for the 1979–2009 simulation period.

large differences in annual values that fundamentally reflect inherent differences in the underlying model methodologies. The degree-day ice growth model is dependent on freezing intensity, in which the effects of both snow cover and streamflow on ice growth were excluded. Differences in the annual ice volumes estimated by the two methods likely represent influences of both snow cover and streamflow on estimated river ice dynamics. The representative examples are shown in the simulation records for the early 1990s and latter 2000s, when SND was positively anomalous.

4) TRENDS

The regional trend map of model-estimated annual maximum ice thickness (Fig. 10c) shows large spatial heterogeneity over the pan-Arctic rivers. The magnitude of the maximum ice thickness trend is generally larger for northern inland rivers than southern ones. Decreasing (increasing) trends in maximum ice thickness generally coincide with increasing (decreasing) trends in model-estimated SND trends (Fig. 10b). The general inverse relationship between model-estimated ice thickness and SND from this study provides insight on how snow cover changes are affecting pan-Arctic river ice phenology. The increasing model SND trends further insulate river ice from the colder atmosphere, promoting warmer temperatures and thinner ice; these effects are particularly apparent for central Siberia and northeastern Canada rivers (Fig. 10c). Areas with decreasing model ice thickness trends represented 64.2% of the pan-Arctic rivers examined (Fig. 10c). However, less insulation by thinning SND trends resulted in thicker ice thickness trends as identified in Alaska rivers.

An estimated earlier ice breakup trend is widespread over the pan-Arctic rivers (Fig. 10d). An earlier ice breakup trend is identified even in cells with increasing ice thickness trends because of the contrasting effects of a shallower snowpack trend, including western North America rivers (Fig. 10c). Thicker river ice may increase resistance and delay spring ice breakup. A shallow snowpack generally promotes a weaker spring flood pulse that is less effective for mechanical ice breakup. However, thinner snow cover is depleted more rapidly in a warmer spring, resulting in a lower estimated river ice albedo that enhances ice decay (Hicks et al. 2009). Despite these opposing processes, the model results indicate a predominantly earlier river ice breakup response to SAT spring warming trends. However,

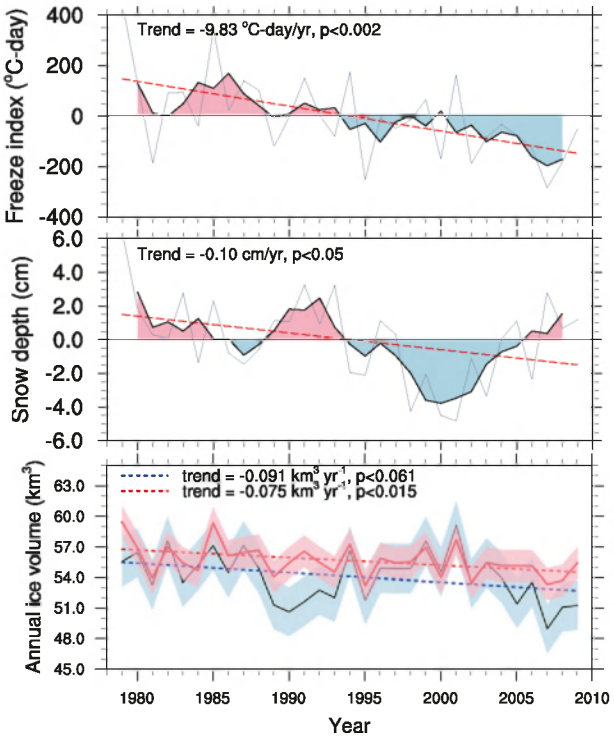

FIG. 9. Time series of (top) anomalous freezing index (October–April), (middle) simulated winter mean snow depth (January–March), and (bottom) total ice volume derived from model-simulated maximum ice thickness (blue) and the degree-day ice growth model (red) over the pan-Arctic rivers. Annual anomalies for freezing index and snow depth represent differences from the 1979–2009 period means. Dashed lines represent the long-term trend over the 1979–2009 record. Shaded areas in (bottom) denote one temporal standard deviation ranges.

unexceptional spring cooling was observed in southern Canada in the recent decade (Bekryaev et al. 2010), which coincides with later model-estimated river ice breakup (Fig. 10d). These results indicate that river ice breakup is closely associated with local spring conditions. A later estimated river ice freezeup trend is also widely distributed over the pan-Arctic (Fig. 10e); the net effect of generally earlier ice breakup in the spring and later ice formation in fall results in generally widespread model trends toward a longer annual ice-free period (Fig. 10f).

c. *Model sensitivity experiments*

Model sensitivity experiments were conducted by varying SAT and precipitation forcings (Table 1) to evaluate seasonally varying impact factors affecting estimated river ice processes. The resulting average differences in estimated annual maximum river ice thickness between the sensitivity experiments and the baseline unadjusted or control simulations is presented in Fig. 11. The model-estimated river ice thickness was sensitive to changes in SND, whereby an increase (decrease) in SND decreased (increased) estimated ice thickness (Figs. 11a,b). The absolute value of ice thickness change was larger when the SND decreased (e.g., Figs. 11, 13a) for average differences between Siberian and North American rivers. Similar results were also found for the sensitivity experiments adjusting October–March precipitation by ±30% (Fig. 14). The magnitude of estimated ice thickness change in the pan-Arctic rivers was larger for the snowfall treatments (i.e., +19.5 and −13.1 cm change in ice thickness for respective snowfall decrease and increase) than for the SAT treatments (Fig. 14). There is a nonlinear relationship between SND and the magnitude of snow insulation, whereby the insulation rate has a minimal impact above a prescribed critical threshold (Park et al. 2015). The model sensitivity experiments projected average changes in maximum river ice thickness of −4.2 and +6.5 cm given respective 10% snowfall increases and decreases.

The estimated maximum river ice thickness decreased (increased) by 2.4 cm for every 1°C increase (decrease) in cold season SAT (Fig. 14). Interestingly, the SAT impact on river ice growth was generally lower than that of SND (Figs. 13a, 14). The estimated river ice growth is completely dependent on SAT without an insulating snow cover layer. In contrast, when snow cover is present over the river ice, the snowpack can further amplify or reduce SAT effects. Therefore, regional snow cover variations may result in river ice trends that are uncorrelated with SAT. These effects are observed for some northern rivers, including $DSUT_{O\_M}$ (Fig. 11e) and $USDT_{O\_M}$ (Fig. 11f), where snow insulation effects evidently overwhelmed the influence of SAT on estimated river ice growth changes (Fig. 13a). In contrast, for southern North America and western Eurasia rivers, where SAT was relatively warm, the estimated ice thickness was largely sensitive to SAT. Although Arctic winter SAT is in a warming state (Bekryaev et al. 2010), Arctic winters still remain extremely cold, especially in more northerly regions. These cold conditions increase model sensitivity of river ice to snow insulation. The combined model experiments ($DSUT_{O\_M}$ and $USDT_{O\_M}$) suggest that ice growth in colder northern rivers is strongly dependent on changes in SND, while SAT has a larger influence on ice phenology in relatively warm southern rivers within the pan-Arctic domain.

The model sensitivity experiments indicate that SAT has a strong effect on river ice breakup dates (Figs. 12, 13b). The model treatment for the 2°C SAT increase during April–May resulted in earlier estimated ice breakup of 10 or more days for northwestern Siberia

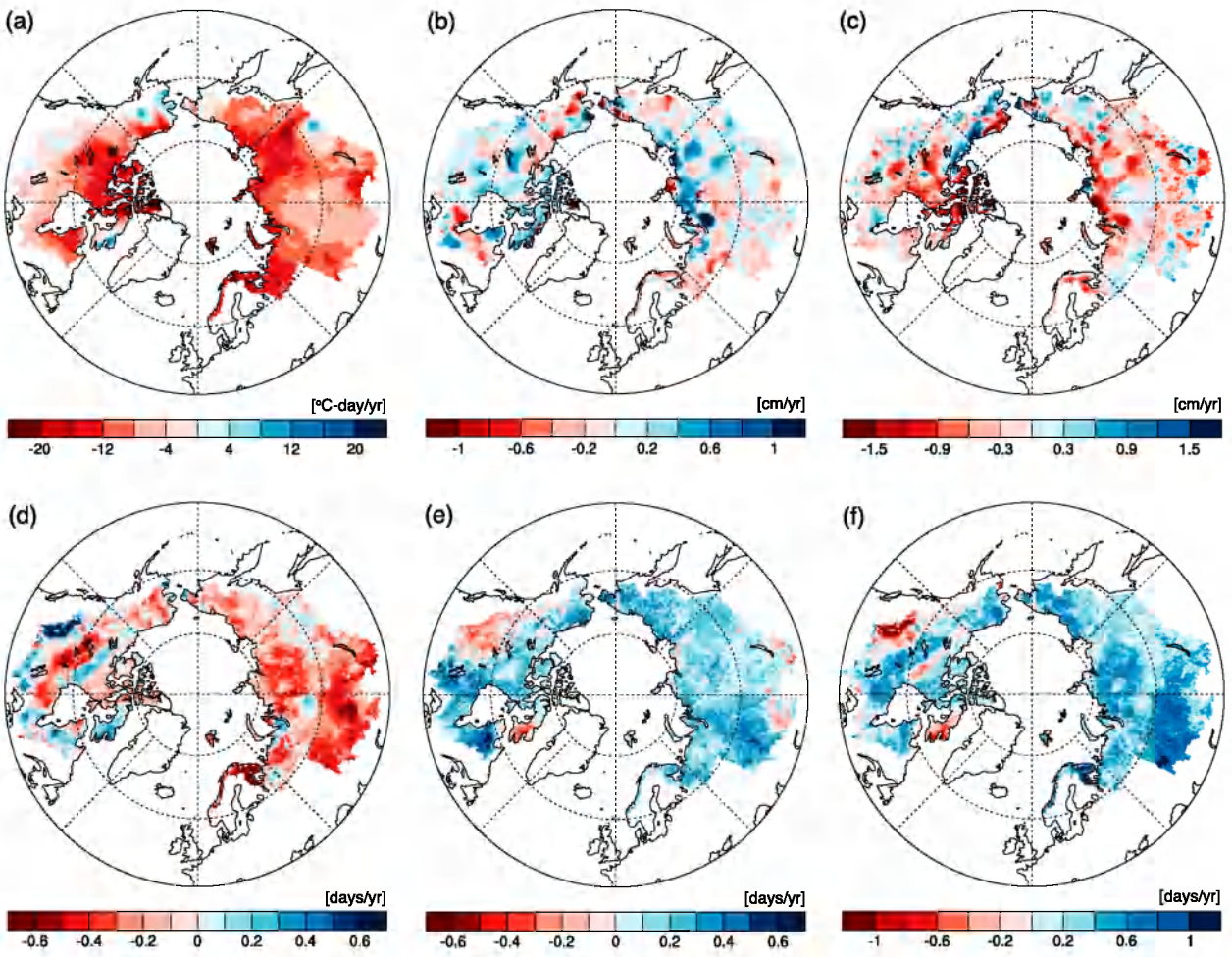

FIG. 10. Model-estimated trend maps for (a) freezing index during October–April, (b) average snow depth for January–March, (c) maximum river ice thickness, (d) ice breakup date, (e) ice freezeup date, and (f) annual ice-free duration over the 1979–2009 simulation period.

rivers (Fig. 12b). The spring SAT increase also advanced seasonal ice breakup in Siberian and North American rivers on average by 6–7 days (Fig. 13b). A previous model sensitivity study revealed a similar 6–10-day earlier ice breakup response to a 2°C uniform increase in SAT for western Siberia rivers (Beltaos and Prowse 2009). Prowse and Bonsal (2004) also noted that a long-term 2°–3°C increase in spring SAT advanced river ice breakup by 10–15 days for Canadian rivers.

River ice thickness during winter also influences spring ice breakup timing. Thicker (thinner) ice development due to decreased (increased) SND delayed (advanced) model-estimated ice breakup (DS_{O_M} and US_{O_M}) (Fig. 13b). The two model experiments (DS_{O_M} and US_{O_M}) partially included the influence of snowmelt discharge on river ice breakup. However, their influence was less than the spring SAT adjustment (i.e., DT_{A_M} and UT_{A_M}) (Fig. 13b). Warming spring SAT led to earlier river ice breakup regardless of prior winter ice thickness conditions ($DS_{O\_M}UT_{A\_M}$ and $US_{O\_M}UT_{A\_M}$) (Fig. 13b). The combined experiments indicate that river ice breakup is strongly dependent on spring SAT. In $DS_{O\_M}UT_{A\_M}$ (Fig. 12c), some southern rivers exhibit unexceptionally later ice breakup than the CTRL. In these areas, ice breakup is largely completed prior to April, and the later breakup trend is attributed to lower SND levels.

d. *Uncertainties in model simulations*

Snow cover formed over river ice likely experiences different conditions relative to adjacent land areas because of variations in terrain, microclimate, and vegetation, including the formation of white ice from the snowpack (Adams and Prowse 1981; Lemmetyinen et al. 2011) and stronger wind on the river surface (Beltaos and Prowse 2009). However, the model-simulated SND

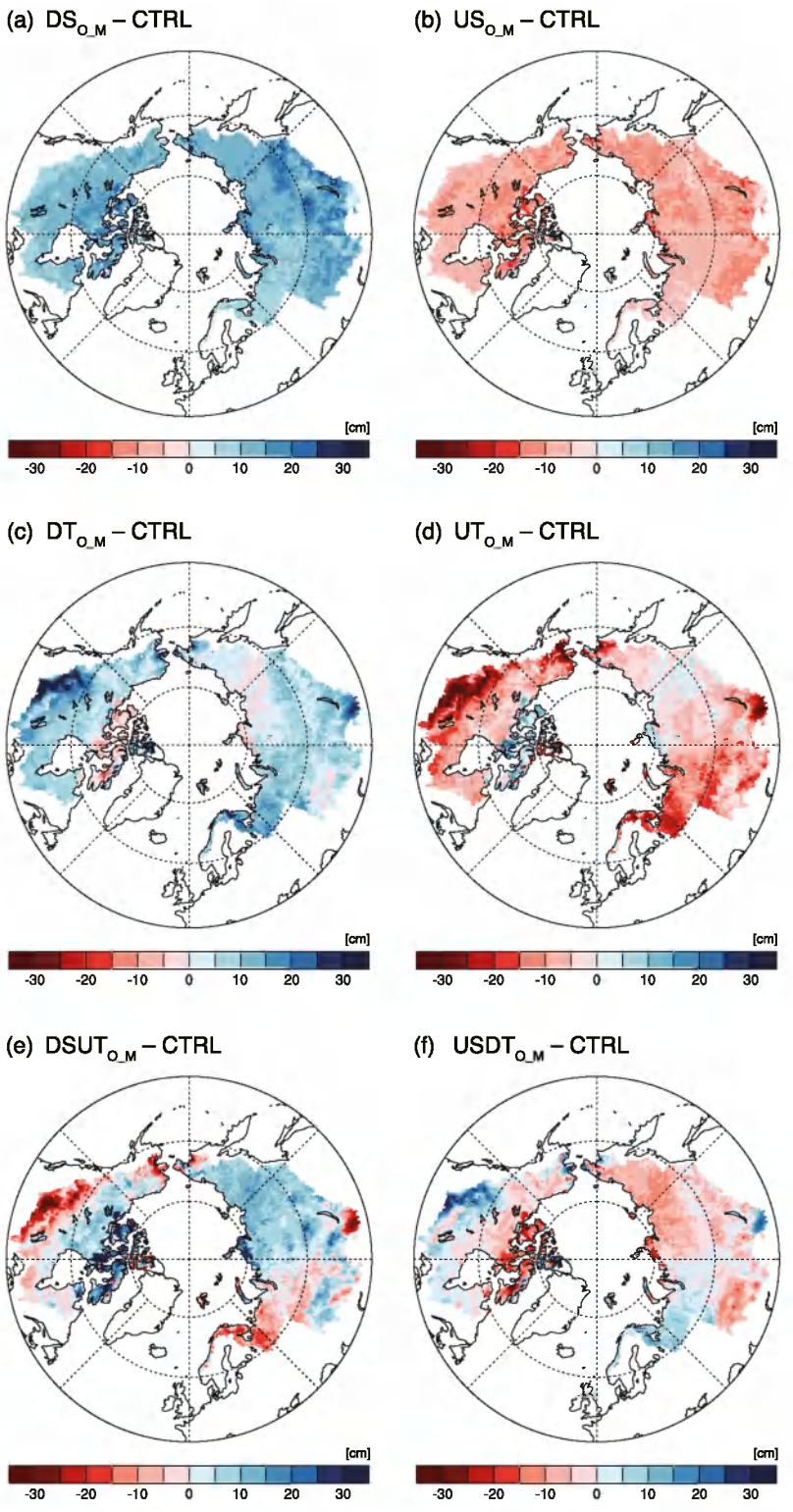

FIG. 11. Average differences in estimated maximum river ice thickness for model experiments (a) DS_{O_M}, (b) US_{O_M}, (c) DT_{O_M}, (d) UT_{O_M}, (e) $DSUT_{O\_M}$, and (f) $USDT_{O\_M}$ against CTRL for the 1979–2009 simulation period.

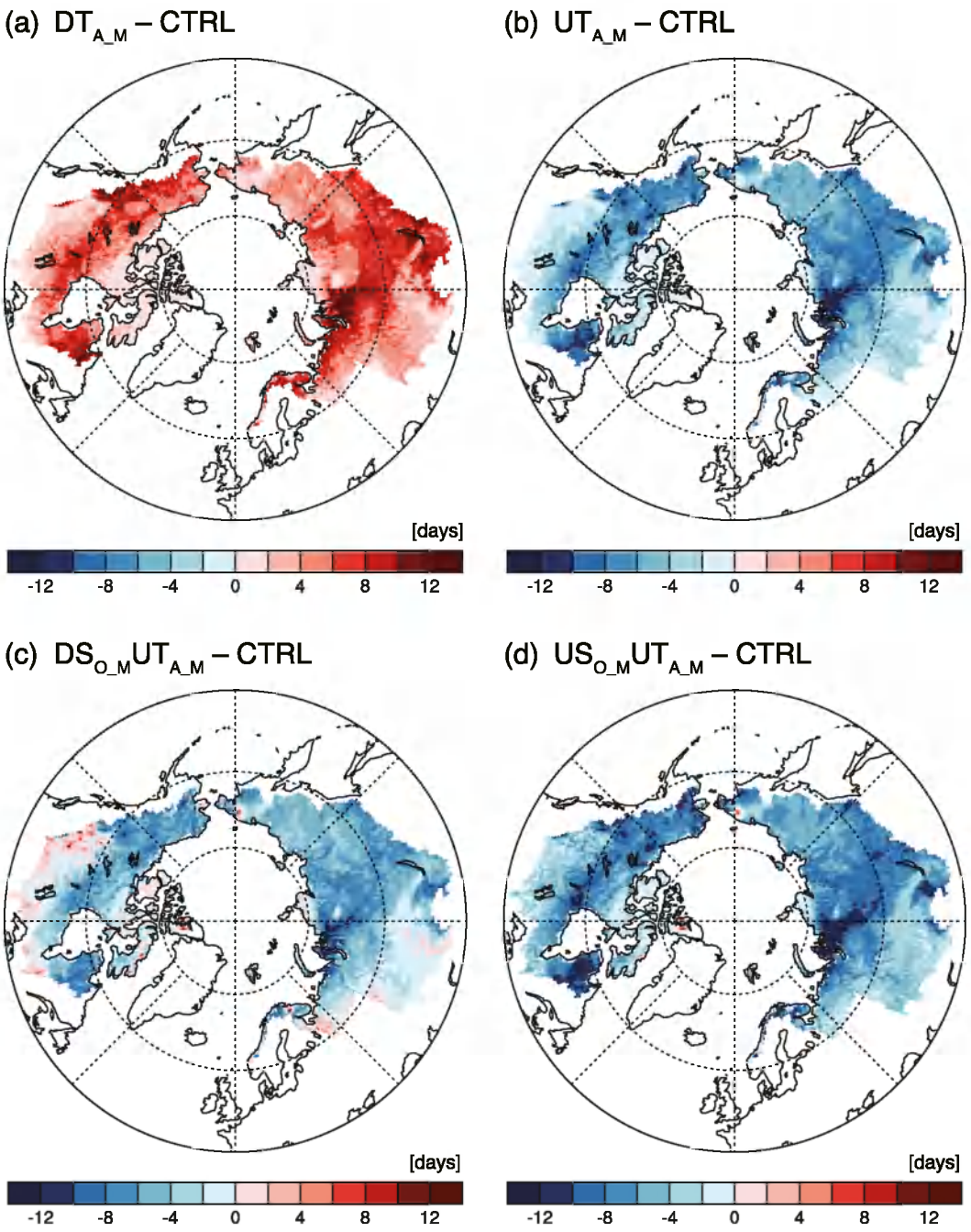

FIG. 12. Average differences in estimated river ice breakup dates for model experiments (a) DT_{A_M}, (b) UT_{A_M}, (c) $DS_{O\_M}UT_{A\_M}$, and (d) $US_{O\_M}UT_{A\_M}$ from CTRL for the 1979–2009 simulation period.

levels used for the comparisons against SND observations over river ice largely represent land conditions around the major river mouths and were generally larger than the observations (Fig. 3). The model also assumed spatially homogeneous SND dynamics between river water bodies and land areas within a grid cell, which may propagate to additional model uncertainties for estimating river ice thickness and volume associated with the SND biases. For example, the increase (decrease) of 30% in winter snowfall increased (decreased) SND by 12.6 (13.0) cm on average over the pan-Arctic (Fig. 14), resulting in a decrease (increase) of 6.0 (9.1) km^3 in estimated maximum mean ice volume relative to the CTRL experiment.

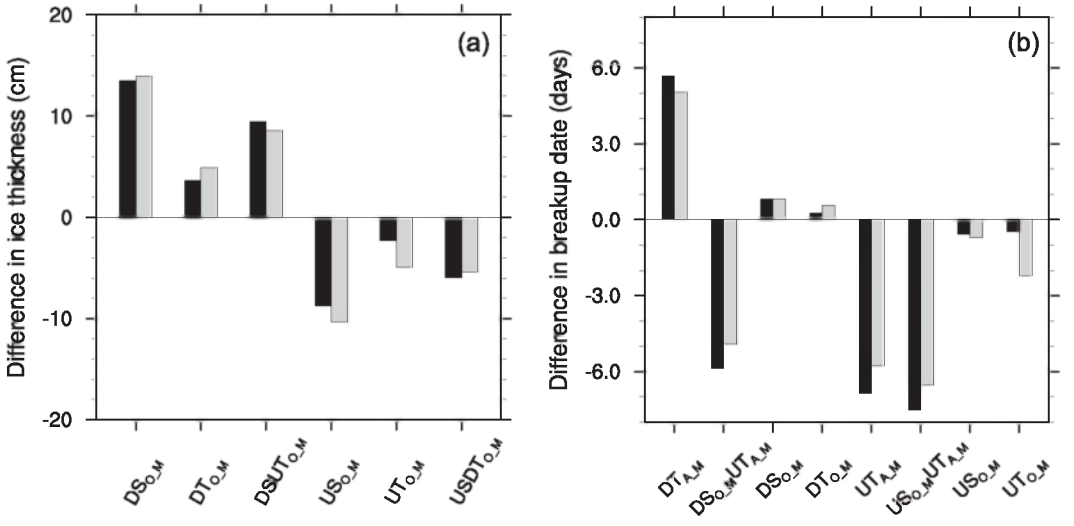

FIG. 13. Differences in estimated (a) maximum ice thickness and (b) ice breakup dates for the individual model experiments from the CTRL for Siberia (black) and North America (gray) rivers, defined in Fig. 7, for the 1979–2009 simulation period.

The CHANGE model requires river length and width information for individual grid cells to determine river ice volume. The river width of individual grid cells was estimated by the annual mean discharge from both the grid cell and the mouth of the river basin (Arora and Boer 1999). The estimation of river width depends on the quality and accuracy of the river discharge calculations and related processes. The model also used a constant width along the river route of individual grid cells, which is uncommon in nature and contributes to uncertainties in model-simulated river ice thickness and volume.

5. Discussion

This study used a physical process model to calculate the total area and maximum volume of ice over all pan-Arctic rivers, including those in the Hudson Bay basin. The river discharge and ice thickness simulations were generally consistent with in situ observations at the mouths and upstream stations of the major Arctic rivers (Figs. 2, 4). The calculated Arctic river ice extent was $0.048 \times 10^6\,km^2$, accounting for 40% of the estimated Northern Hemisphere river ice extent ($0.12 \times 10^6\,km^2$; Brooks et al. 2013). The estimated pan-Arctic river ice extent has a smaller areal extent than the Greenland ice sheet ($1.7 \times 10^6\,km^2$; Bamber and Layberry 2001) and the mean August snow extent ($1.9 \times 10^6\,km^2$) on land across the Northern Hemisphere (Lemke et al. 2007). The model-calculated mean maximum annual river ice volume of $54.1\,km^3$ represented 39% of the total estimated river ice volume of the Northern Hemisphere (Brooks et al. 2013). The estimated pan-Arctic river ice volume decreased by $2.82\,km^3$ or 0.5% of mean annual volume over the 1979–2009 record (Fig. 9). The estimated decrease in river ice volume is considerably smaller than the mass loss from Arctic glaciers and ice caps, which has been estimated to be $7.3\,km^3\,yr^{-1}$ from 1985–2003 (AMAP 2011). However, to our knowledge, our assessment of regional ice changes for pan-Arctic rivers is a first comprehensive analysis of river ice dynamics using a numerical model. Our results also indicate that regional change in river ice volume and thickness is more significantly correlated with SND than winter SAT changes (Figs. 7, 11), which contrasts with previous studies indicating a dominant SAT control (e.g., Michel 1971).

The maximum ice volume of the six major Arctic rivers (Ob, Yenisey, Lena, Kolyma, Yukon, and Mackenzie) accounted for 60.8% of the estimated mean annual volume of $54.1\,km^3$ over the entire pan-Arctic domain (Fig. 15). The contribution of individual rivers to the total estimated pan-Arctic river ice volume is generally proportional to basin size, but with significant variability in the contributions from some basins of similar size. For example, the Yenisey and Lena have similar basin areas but markedly different river ice contributions to the total estimated river ice volume. Relative differences in the ice contributions of similarly sized basins largely reflects spatial heterogeneity in regional climate, terrain, vegetation, and associated SND regimes among basins. The different contribution levels

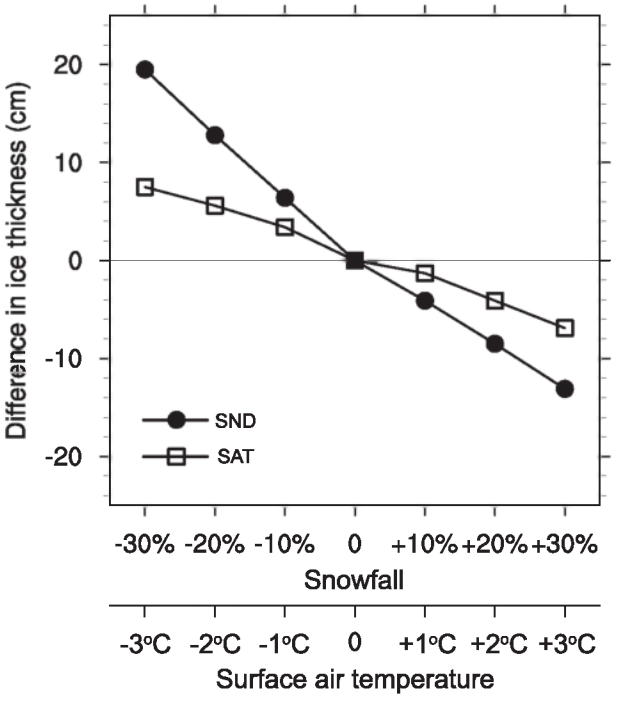

FIG. 14. Sensitivity of estimated maximum river ice thickness to changes in overlying snowfall (circles) and surface air temperature (squares) during October–March. The values reported from the individual model experiments are averaged over the pan-Arctic river systems defined in Fig. 1. The calculation was done by the same method used in Figs. 7 and 8 on the basis of the annual differences in individual grid cells between the model experiments and the control for the 1979–2009 period.

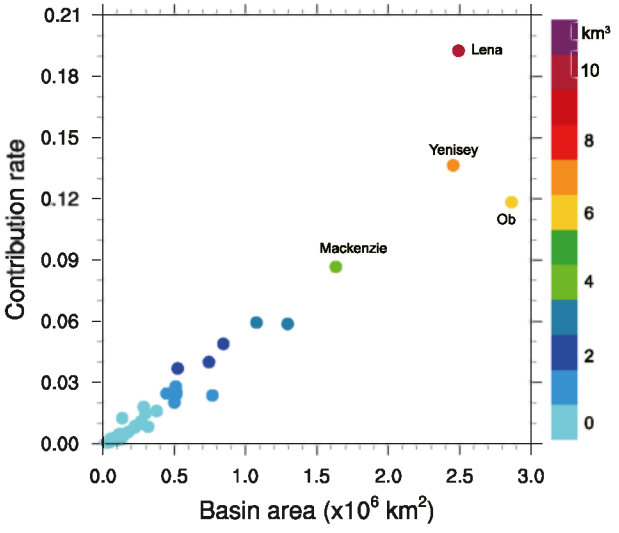

FIG. 15. Comparison of contribution rates of river ice volume from basins with different climates and watershed areas (Fig. 1) to the average total maximum ice volume 54.1 km^3 over the pan-Arctic rivers. Colors denote estimated average river ice volume contributed by individual basins over the 1979–2009 period.

between the Yenisey and Lena reflect different SAT and SND conditions between these basins (Fig. 3). Higher winter low flows may also contribute to lower ice volume in the Yenisey (Fig. 2). The Ob has the largest basin area but a lower ice contribution than the Yenisey and Lena, which may reflect thinning of estimated river ice from winter SAT warming and deeper SND trends within the Ob basin. Differences in river ice volume are also evident between smaller basins with similar areas (Fig. 15).

The Arctic warming trend resulted in large changes in estimated snow cover and SND properties. The autumn-to-spring snow season length was shortened. However, large regional SND variability shows general decreasing trends in western North America (Dyer and Mote 2006) and increasing trends in Siberia (Bulygina et al. 2009; Park et al. 2013b). Deepening Siberian snow cover trends resulted in decreases in estimated river ice thickness due to increases in snow cover insulation (Fig. 7). The simulated 0.3 cm yr^{-1} decrease in mean regional ice thickness (Fig. 7) is similar to reported decreases (-1.26 to -0.08 cm yr^{-1}) observed at the mouths of Siberian rivers (Shiklomanov and Lammers 2014). It has been projected that snow water equivalent in the Siberia sector will increase with future climate change (Brown and Mote 2009). The reported and projected snow trends, including our results, suggest that increasing SND levels will promote further decreases in pan-Arctic river ice thickness.

Future climate warming is likely to further advance the timing of ice breakup. Andrishak and Hicks (2008), applying a one-dimensional hydrodynamic model to the Town of Peace River, projected that ice breakup in the 2050s would be 15 days earlier under the SRES A2 climate projection scenario. Continuing spring warming trends could change spatial climatic gradients between basin headwaters and downstream reaches, which could alter the timing of ice breakup and associated flooding. A suite of global climate models projected that some large Arctic-flowing rivers in Russia will experience relatively large spring (March–April) warming in their downstream reaches and a reduction in the controlling climatic gradient (Prowse et al. 2006). Prowse and Bonsal (2004) reported the northward shift of an ice-regime-defined temperate zone of North America, where midwinter breakup occurs on occasion with a 6°C warming of mean winter temperatures. Such a dramatic northward shift of the temperate zone is not evident at this time. During this century, however, a 6°C winter warming is presumably likely, as reported by the IPCC AR5, whereby pan-Arctic rivers will become susceptible to more frequent flooding and ice breakup events.

One of the significant changes in river environments affected by a longer ice-free season may be T_w. Earlier ice breakup likely results in warmer T_w combined with warmer spring SAT. Water temperature T_w exhibits abrupt increases following ice breakup (Fig. 6). In the case of Siberian rivers, T_w increased by 1°–2°C in the first 10 days following ice breakup (Fig. 6). A calculation from this result suggests that an increase of 0.2°C day^{-1} in early spring would increase the river heat flux by 0.013 to 0.084 TW under a discharge of 15 000 to 100 000 m^3 s^{-1}. The heat flux H (W) was calculated by $H = \rho C_p T_w Q$, where ρ is water density (kg m^{-3}), C_p is specific heat capacity (J kg^{-1} °C^{-1}), and Q is river discharge (m^3 s^{-1}). Arctic-flowing monthly mean heat fluxes of Siberian rivers (e.g., Yenisey, Lena, and Kolyma) are <0.1 TW in May (Whitefield et al. 2015). The estimated (0.013–0.084 TW) heat flux increase is expected to contribute to warmer T_w levels and additional energy inputs to the Arctic Ocean heat content, potentially impacting Arctic sea ice and atmosphere dynamics (Yang et al. 2014; Whitefield et al. 2015). The apparent rates of T_w warming (Fig. 6) and discharge increases during the early spring are considerable (Fig. 2). Furthermore, SAT records indicate strong warming trends in the spring. Thus, the impact of earlier ice breakup on spring T_w warming is likely larger than our simulations indicate.

6. Conclusions

The problem of decreasing gauging and ground-based observations of Arctic rivers has made it more difficult to conduct basic hydrological research in cold regions (Shiklomanov et al. 2002). Numerical modeling, in conjunction with satellite remote sensing and other ancillary data, provides a means for spatial and temporal extrapolation of sparse ground observations and identifying regional hot spots requiring more detailed observations and process investigations. Model simulation experiments also provide an efficient way to diagnose underlying processes and interactive effects driving observed changes. The model framework described in this study includes a detailed land process model (CHANGE) coupled with other models of river ice and T_w dynamics, runoff routing, and river discharge. The resulting framework provides a model advancement that can quantitatively assess changes in river ice phenology, thickness, and volume over the major pan-Arctic rivers. The model results indicate that ice thickness and volume over the pan-Arctic rivers decreased over the 1979–2009 record. The estimated decrease in river ice is more significantly correlated with SND than SAT changes. The timing of annual ice breakup has generally advanced in conjunction with SAT warming in the spring. These findings were verified by model sensitivity experiments based on various scenarios of SAT and cold season precipitation forcings. Ice floes formed by river ice breakup move downstream. In this process, ice jams occur and can induce flooding. However, CHANGE was not yet sufficiently advanced to describe ice jam processes. One of the biggest issues in cold lands hydrology is to know where and when ice jams form and release. Therefore, the improvement of ice-jamming-related processes is a priority for our future work.

Acknowledgments. This work was supported in part by JAMSTEC, the RIHN Research Project C-07, and the Ministry of Education, Science, Sports and Culture, Grant-in-Aid for Scientists (C) 26340018 and (A) 26242026 and for Young Scientists (B) 26870023. Support for University of Montana researchers was provided by NASA (NNX11AP68A and NNX14AB20A).

REFERENCES

Adam, J. C., and D. P. Lettenmaier, 2003: Adjustment of global gridded precipitation for systematic bias. *J. Geophys. Res.*, **108**, 4257, doi:10.1029/2002JD002499.

——, E. A. Clark, D. P. Lettenmaier, and E. F. Wood, 2006: Correction of global precipitation for orographic effects. *J. Climate*, **19**, 15–38, doi:10.1175/JCLI3604.1.

Adams, W. P., and T. D. Prowse, 1981: Evolution and magnitude of spatial patterns in the winter cover of temperate lakes. *Fennia*, **159**, 343–359.

AMAP, 2011: Snow, Water, Ice and Permafrost in the Arctic (SWIPA): Climate change and the cryosphere. Arctic Monitoring and Assessment Programme Rep., 538 pp. [Available online at http://www.amap.no/documents/doc/snow-water-ice-and-permafrost-in-the-arctic-swipa-climate-change-and-the-cryosphere/743.]

Andrishak, R., and F. Hicks, 2008: Simulating the effects of climate change on the ice regime of the Peace River. *Can. J. Civ. Eng.*, **35**, 461–472, doi:10.1139/L07-129.

Arora, V. K., and G. J. Boer, 1999: A variable velocity flow routing algorithm for GCMs. *J. Geophys. Res.*, **104**, 30 965–30 979, doi:10.1029/1999JD900905.

Bamber, J. L., and R. L. Layberry, 2001: A new ice thickness and bed data set for the Greenland ice sheet: 1. Measurement, data reduction, and errors. *J. Geophys. Res.*, **106**, 33 773–33 780, doi:10.1029/2001JD900054.

Bekryaev, R. V., I. V. Polyakov, and V. A. Alexeev, 2010: Role of polar amplification in long-term surface air temperature variations and modern Arctic warming. *J. Climate*, **23**, 3888–3906, doi:10.1175/2010JCLI3297.1.

Beltaos, S., 1997: Onset of river ice breakup. *Cold Reg. Sci. Technol.*, **25**, 183–196, doi:10.1016/S0165-232X(96)00011-0.

——, and T. Prowse, 2009: River-ice hydrology in a shrinking cryosphere. *Hydrol. Processes*, **23**, 122–144, doi:10.1002/hyp.7165.

Benson, B., and J. Magnuson, 2012: Global lake and river ice phenology database. National Snow and Ice Data Center, accessed 15 May 2015, doi:10.7265/N5W66HP8.

Bieniek, P. A., U. S. Bhatt, L. A. Rundquist, S. D. Lindsey, X. Zhang, and R. L. Thoman, 2011: Large-scale climate controls of interior Alaska river ice breakup. *J. Climate*, **24**, 286–297, doi:10.1175/2010JCLI3809.1.

Brooks, R. N., T. D. Prowse, and I. J. O'Connell, 2013: Quantifying Northern Hemisphere freshwater ice. *Geophys. Res. Lett.*, **40**, 1128–1131, doi:10.1002/grl.50238.

Brown, R. D., and P. W. Mote, 2009: The response of Northern Hemisphere snow cover to a changing climate. *J. Climate*, **22**, 2124–2145, doi:10.1175/2008JCLI2665.1.

Bulygina, O., V. Razuvaev, and N. Korshunova, 2009: Change in snow cover over northern Eurasia in the last decades. *Environ. Res. Lett.*, **4**, 045026, doi:10.1088/1748-9326/4/4/045026.

Decharme, B., and H. Douville, 2006: Uncertainties in the GSWP-2 precipitation forcing and their impacts on regional and global hydrological simulations. *Climate Dyn.*, **27**, 695–713, doi:10.1007/s00382-006-0160-6.

Dyer, T., and T. Mote, 2006: Spatial variability and trends in observed snow depth over North America. *Geophys. Res. Lett.*, **33**, L16503, doi:10.1029/2006GL027258.

Gatto, L. W., 1990: Monitoring river ice with Landsat images. *Remote Sens. Environ.*, **32**, 1–16, doi:10.1016/0034-4257(90)90094-3.

Gray, D. M., and T. D. Prowse, 1993: Snow and floating ice. *Handbook of Hydrology*, 1st ed. D. R. Maidment, Eds., McGraw-Hill, 7.1–7.58.

Hatta, S., H. Hayakawa, H. Park, T. Yamazaki, K. Yamamoto, and T. Ohta, 2009: Long term runoff analysis of the Lena River basin using a distributed hydrological model. *J. Japan Soc. Hydrol. Water Resour.*, **22**, 177–187, doi:10.3178/jjshwr.22.177.

Hicks, F., W. Cui, and G. Ashton, 2009: Heat transfer and ice cover decay. *River Ice Breakup*, S. Beltaos, Ed., Water Resources Publications, 67–124.

IPCC, 2013: *Climate Change 2013: The Physical Science Basis*. Cambridge University Press, 1535 pp, doi:10.1017/CBO9781107415324.

Kim, Y., J. S. Kimball, K. Zhang, and K. C. McDonald, 2012: Satellite detection of increasing Northern Hemisphere non-frozen seasons from 1979 to 2008: Implications for regional vegetation growth. *Remote Sens. Environ.*, **121**, 472–487, doi:10.1016/j.rse.2012.02.014.

——, ——, ——, K. Didan, I. Velicogna, and K. C. McDonald, 2014: Attribution of divergent northern vegetation growth responses to lengthening non-frozen seasons using satellite optical-NIR and microwave remote sensing. *Int. J. Remote Sens.*, **35**, 3700–3721, doi:10.1080/01431161.2014.915595.

——, ——, D. A. Robinson, and C. Derksen, 2015: New satellite climate data records indicate strong coupling between recent frozen season changes and snow cover over high northern latitudes. *Environ. Res. Lett.*, **10**, 084004, doi:10.1088/1748-9326/10/8/084004.

Kimball, J. S., K. C. McDonald, A. R. Keyser, S. Frolking, and S. W. Running, 2001: Application of the NASA scatterometer (NSCAT) for determining the daily frozen and nonfrozen landscape of Alaska. *Remote Sens. Environ.*, **75**, 113–126, doi:10.1016/S0034-4257(00)00160-7.

Lammers, R. B., J. W. Pundsack, and A. I. Siklomanov, 2007: Variability in river temperature, discharge, and energy flux from the Russian pan-Arctic landmass. *J. Geophys. Res.*, **112**, G04S59, doi:10.1029/2006JG000370.

Lemke, P., and Coauthors, 2007: Observations: Changes in snow, ice and frozen ground. *Climate Change 2007: The Physical Science Basis*, S. Solomon et al., Eds., Cambridge University Press, 337–383. [Available online at https://www.ipcc.ch/pdf/assessment-report/ar4/wg1/ar4-wg1-chapter4.pdf.]

Lemmetyinen, J., A. Kontu, J. Karna, J. Vehvilainen, M. Takala, and J. Pulliainen, 2011: Correcting for the influence of frozen lakes in satellite microwave radiometer observations through application of a microwave emission model. *Remote Sens. Environ.*, **115**, 3695–3706, doi:10.1016/j.rse.2011.09.008.

Lesack, L. F. W., P. Marsh, F. E. Hicks, and D. L. Forbes, 2014: Local spring warming drives earlier river-ice breakup in a large Arctic delta. *Geophys. Res. Lett.*, **41**, 1560–1566, doi:10.1002/2013GL058761.

Ma, X., and Y. Fukushima, 2002: A numerical model of the river freezing process and its application to the Lena River. *Hydrol. Processes*, **16**, 2131–2140, doi:10.1002/hyp.1146.

Magnuson, J. J., and Coauthors, 2000: Historical trends in lake and river ice cover in the Northern Hemisphere. *Science*, **289**, 1743–1746, doi:10.1126/science.289.5485.1743.

Michel, B., 1971: *Winter Regime of Rivers and Lakes. Cold Reg. Sci. Eng. Monogr.*, III-B1a, U.S. Army Cold Regions Research and Engineering Laboratory, 139 pp. [Available online at http://acwc.sdp.sirsi.net/client/en_US/search/asset/1011701.]

Murphy, M. A., I. P. Martini, and R. Rrotz, 2001: Seasonal changes in subarctic wetlands and river ice breakup detectable on RADARSAT images, southern Hudson Bay Lowland, Ontario, Canada. *Can. J. Remote Sens.*, **27**, 143–158, doi:10.1080/07038992.2001.10854928.

Ngo-Duc, T., T. Oki, and S. Kanae, 2007: A variable streamflow velocity method for global river routing model: Model description and preliminary results. *Hydrol. Earth Syst. Sci. Discuss.*, **4**, 4389–4414, doi:10.5194/hessd-4-4389-2007.

Oki, T., and Y. C. Sud, 1998: Design of Total Runoff Integrating Pathways (TRIP)—A global river channel network. *Earth Interact.*, **2**, 1–37, doi:10.1175/1087-3562(1998)002<0001:DOTRIP>2.3.CO;2.

Pappenberger, F., H. L. Cloke, G. Balsamo, T. Ngo-Duc, and T. Oki, 2010: Global runoff routing with the hydrological component of the ECMWF NWP system. *Int. J. Climatol.*, **30**, 2155–2174, doi:10.1002/joc.2028.

Park, H., Y. Iijima, H. Yabuki, T. Ohta, J. Walsh, Y. Kodama, and T. Ohata, 2011: The application of a coupled hydrological and biogeochemical model (CHANGE) for modeling of energy, water, and CO_2 exchanges over a larch forest in eastern Siberia. *J. Geophys. Res.*, **116**, D15102, doi:10.1029/2010JD015386.

——, H. Yabuki, and T. Ohata, 2012: Analysis of satellite and model datasets for variability and trends in Arctic snow extent and depth, 1948–2006. *Polar Sci.*, **6**, 23–37, doi:10.1016/j.polar.2011.11.002.

——, J. E. Walsh, A. N. Fedorov, A. B. Sherstiukov, Y. Iijima, and T. Ohata, 2013a: The influence of climate and hydrological variables on opposite anomaly in active-layer thickness between Eurasian and North America watersheds. *Cryosphere*, **7**, 631–645, doi:10.5194/tc-7-631-2013.

——, ——, Y. Kim, T. Nakai, and T. Ohata, 2013b: The role of declining Arctic sea ice in recent decreasing terrestrial Arctic snow depths. *Polar Sci.*, **7**, 174–187, doi:10.1016/j.polar.2012.10.002.

——, A. N. Fedorov, M. N. Zheleznyak, P. Y. Konstantinov, and J. E. Walsh, 2015: Effect of snow cover on pan-Arctic permafrost thermal regimes. *Climate Dyn.*, **44**, 2873–2895, doi:10.1007/s00382-014-2356-5.

Pavelsky, T. M., and L. C. Smith, 2004: Spatial and temporal patterns in Arctic river ice breakup observed with MODIS and AVHRR time series. *Remote Sens. Environ.*, **93**, 328–338, doi:10.1016/j.rse.2004.07.018.

Prowse, T. D., and F. M. Conly, 1998: Effects of climate variability and flow regulation on ice-jam flooding of a northern delta. *Hydrol. Processes*, **12**, 1589–1610, doi:10.1002/(SICI)1099-1085(199808/09)12:10/11<1589::AID-HYP683>3.0.CO;2-G.

——, and S. Beltaos, 2002: Climatic control of river-ice hydrology: A review. *Hydrol. Processes*, **16**, 805–822, doi:10.1002/hyp.369.

——, and B. R. Bonsal, 2004: Historical trends in river-ice breakup: A review. *Hydrol. Res.*, **35**, 281–293.

——, F. J. Wrona, J. Reist, J. J. Gibson, J. E. Hobbie, L. M. J. Levesque, and W. Vincent, 2006: Climate change effects on hydroecology of Arctic freshwater ecosystems. *Ambio*, **35**, 347–358, doi:10.1579/0044-7447(2006)35[347:CCEOHO]2.0.CO;2.

Ramankutty, R., and J. A. Foley, 1999: Estimating historical changes in global land cover: Croplands from 1700 to 1992. *Global Biogeochem. Cycles*, **13**, 997–1027, doi:10.1029/1999GB900046.

Rawlins, M. A., K. C. McDonald, S. Frolking, R. B. Lammers, M. Fahnestock, J. S. Kimball, and C. J. Vörösmarty, 2005: Remote sensing of snow thaw at the pan-Arctic scale using the SeaWinds scatterometer. *J. Hydrol.*, **312**, 294–311, doi:10.1016/j.jhydrol.2004.12.018.

——, H. Ye, D. Yang, A. Shiklomanov, and K. C. McDonald, 2009: Divergence in seasonal hydrology across northern Eurasia: Emerging trends and waster cycle linkages. *J. Geophys. Res.*, **114**, D18119, doi:10.1029/2009JD011747.

Screen, J. A., and I. Simmonds, 2010: The central role of diminishing sea ice in recent Arctic temperature amplification. *Nature*, **464**, 1334–1337, doi:10.1038/nature09051.

Semmens, K. A., and J. M. Ramage, 2013: Recent changes in spring snowmelt timing in the Yukon River basin detected by passive microwave satellite data. *Cryosphere*, **7**, 905–916, doi:10.5194/tc-7-905-2013.

Serreze, M. C., D. H. Bromwich, M. P. Clark, A. J. Etringer, T. Zhang, and R. Lammers, 2002: Large-scale hydro-climatology of the terrestrial Arctic drainage system. *J. Geophys. Res.*, **108**, 8160, doi:10.1029/2001JD000919.

Shiklomanov, A. I., and R. B. Lammers, 2014: River ice responses to a warming Arctic—Recent evidence from Russian rivers. *Environ. Res. Lett.*, **9**, 035008, doi:10.1088/1748-9326/9/3/035008.

——, ——, and C. J. Vorosmarty, 2002: Widespread decline in hydrological monitoring threatens pan-Arctic research. *Eos, Trans. Amer. Geophys. Union*, **83**, 13–17, doi:10.1029/2002EO000007.

Slater, A. G., T. J. Bohn, J. L. McCreight, M. C. Serreze, and D. P. Lettenmaier, 2007: A multimodel simulation of pan-Arctic hydrology. *J. Geophys. Res.*, **112**, G04S45, doi:10.1029/2006JG000303.

Smith, L. C., T. M. Pavelsky, G. M. MacDonald, A. I. Shiklomanov, and R. B. Lammers, 2007: Rising minimum daily flows in northern Eurasian rivers: A growing influence of groundwater in the high-latitude hydrologic cycle. *J. Geophys. Res.*, **112**, G04S47, doi:10.1029/2006JG000327.

Su, F., J. C. Adam, L. C. Bowling, and D. P. Lettenmaier, 2005: Streamflow simulations of the terrestrial Arctic domain. *J. Geophys. Res.*, **110**, D08112, doi:10.1029/2004JD005518.

Thornton, P. E., and N. E. Zimmermann, 2007: An improved canopy integration scheme for a land surface model with prognostic canopy structure. *J. Climate*, **20**, 3902–3923, doi:10.1175/JCLI4222.1.

Van Vliet, M. T. H., J. R. Yearsley, W. H. P. Franssen, F. Ludwig, I. Haddeland, D. P. Lettenmaier, and P. Kabat, 2012: Coupled daily streamflow and water temperature modeling in large river basin. *Hydrol. Earth Syst. Sci.*, **16**, 4303–4321, doi:10.5194/hess-16-4303-2012.

Vincent, F., D. Raucoules, T. Degroeve, G. Edwards, and M. Abolfazi Mostafavi, 2004: Detection of river/sea ice deformation using satellite interferometry: Limits and potential. *Int. J. Remote Sens.*, **25**, 3555–3571, doi:10.1080/01431160410001688303.

Vuglinsky, V. S., 2006: Ice regime in the rivers of Russia, its dynamics during last decades and possible future changes. *Proc. 18th IAHR International Symposium on Ice*, Sapporo, Japan, Nakanishi Publishing Co., Ltd., 93–98.

Weedon, G. P., G. Balsamo, N. Bellouin, S. Gomes, M. J. Best, and P. Viterbo, 2014: The WFDEI meteorological forcing data set: WATCH forcing data methodology applied to ERA-Interim reanalysis data. *Water Resour. Res.*, **50**, 7505–7514, doi:10.1002/2014WR015638.

Whitefield, J., P. Winsor, J. McClelland, and D. Menemenlis, 2015: A new river discharge and river temperature climatology data set for the pan-Arctic region. *Ocean Modell.*, **88**, 1–15, doi:10.1016/j.ocemod.2014.12.012.

Wu, H., J. S. Kimball, M. M. Elsner, N. Mantua, R. F. Adler, and J. Stanford, 2012: Projected climate change impacts on the hydrology and temperature of Pacific Northwest rivers. *Water Resour. Res.*, **48**, W11530, doi:10.1029/2012WR012082.

Yang, D., B. Ye, and A. Shiklomanov, 2004: Discharge characteristics and changes over the Ob River watershed in Siberia. *J. Hydrometeor.*, **5**, 595–610, doi:10.1175/1525-7541(2004)005<0595:DCACOT>2.0.CO;2.

——, P. Marsh, and S. Ge, 2014: Heat flux calculations for Mackenzie and Yukon Rivers. *Polar Sci.*, **8**, 232–241, doi:10.1016/j.polar.2014.05.001.

Yoshikawa, Y., Y. Watanabe, and A. Itoh, 2014: A simple equation for ice sheet thickness and ice formation/breakup prediction. *J. JSCE*, **2**, 203–213, doi:10.2208/journalofjsce.2.1_203.